REPORT DOCUMENTATION PAGE

Form Approved
OMB No. 0704-0188

1. REPORT DATE (DD-MM-YYYY)	2. REPORT TYPE	3. DATES COVERED (From - To)
27-08-2005	Final Technical	01-01-2003 - 31-12-2005

4. TITLE AND SUBTITLE
Filtered Mass Density Function for Subgrid Scale Modeling of Turbulent Diffusion Flames

5a. CONTRACT NUMBER

5b. GRANT NUMBER
F49620-03-1-0022

5c. PROGRAM ELEMENT NUMBER
61102F

6. AUTHOR(S)
P. Givi, M.R.H. Sheikhi, T.G. Drozda and C.K. Madnia

5d. PROJECT NUMBER
2308

5e. TASK NUMBER
BX

5f. WORK UNIT NUMBER

7. PERFORMING ORGANIZATION NAME(S) AND ADDRESS(ES)
Department of Mechanical Engineering
University of Pittsburgh
Pittsburgh, PA 15261

8. PERFORMING ORGANIZATION REPORT NUMBER

9. SPONSORING / MONITORING AGENCY NAME(S) AND ADDRESS(ES)
AFOSR/NA
875 Randolph Street
Suite 325, Room 3112
Arlington, VA 22203
Dr. Julian Tishkoff

10. SPONSOR/MONITOR'S ACRONYM(S)

11. SPONSOR/MONITOR'S REPORT NUMBER(S)

12. DISTRIBUTION / AVAILABILITY STATEMENT
Approved for public release, distribution is unlimited.

AFRL-SR-AR-TR-06-0142

13. SUPPLEMENTARY NOTES

14. ABSTRACT

This research was primarily concentrated on the following issues: (1) development of the joint velocity-scalar filtered density function for subgrid scale (SGS) closure of turbulent combustion; and (2) implementation of the scalar filtered density function for large eddy simulation of complex turbulent flames. An extensive systematic study was performed and resulted in significant new findings. With regard to (1), a modelled transport equation was developed and solved for the joint density function. The predicted results via this model were more accurate than other existing SGS models. With regard to (2), the model was employed for prediction of a piloted jet diffusion flame and a bluff-body stabilized flame. The predicted results compared very well with experimental data.

15. SUBJECT TERMS
Large eddy simulation, turbulent combustion, subgrid scale modeling, filtered density function.

16. SECURITY CLASSIFICATION OF:			17. LIMITATION OF ABSTRACT	18. NUMBER OF PAGES	19a. NAME OF RESPONSIBLE PERSON
a. REPORT	b. ABSTRACT	c. THIS PAGE			Julian M. Tishkoff
unclassified	unclassified	unclassified	UL	46	19b. TELEPHONE NUMBER (include area code) (703) 696-8478

Filtered Mass Density Function for Subgrid Scale Modeling of Turbulent Diffusion Flames

P. Givi, M.R.H. Sheikhi, T.G. Drozda and C.K. Madnia
Department of Mechanical Engineering
University of Pittsburgh
Pittsburgh, PA 15261USA

Abstract

This research was primarily concentrated on the following issues: (1) development of the joint velocity-scalar filtered density function for subgrid scale (SGS) closure of turbulent combustion; and (2) implementation of the scalar filtered density function for large eddy simulation of complex turbulent flames. An extensive systematic study was performed and resulted in significant new findings. With regard to (1), a modelled transport equation was developed and solved for the joint density function. The predicted results via this model were more accurate than other existing SGS models. With regard to (2), the model was employed for prediction of a piloted jet diffusion flame and a bluff-body stabilized flame. The predicted results compared very well with experimental data.

Contents

1 Introduction

It now is recognized widely that one of the most convenient means of predicting the unsteady physics of turbulent reacting flows is via large eddy simulation (LES) [25, 37, 67]. A serious issue in such simulations is accurate modeling of the subgrid scale (SGS) quantities. While this issue is important in any LES, it is particularly difficult when dealing with reacting flows [37, 67, 5].

The predictive capability of probability density function (PDF) methods in Reynolds averaged simulation (RAS) is established very well [67, 19, 32]. This capability is due to the inherent property of the PDF to include the complete statistical information about its variables. It appears that the use of PDF methods for SGS modeling was suggested first by Givi [24]; however, it was the formal definition of the "filtered density function" (FDF) by Pope [65] that facilitated the implementation of LES via PDF. One of the first implementations of LES/FDF was reported by Madnia and Givi [47] in which the shape of the FDF was specified *a priori*. This "presumed FDF" procedure was pursued in several subsequent studies, in most of which it was assumed that the thermo-chemical variables depend on only the mixture fraction, *e.g.* infinitely fast reaction, equilibrium chemistry, *etc.* Therefore, the FDF is univariate [47, 11, 71, 39, 15, 16, 18, 40]. For LES of non-equilibrium reactive flows, it is necessary to assume the "joint" FDF of multi-scalars [20, 21]. All of the assumed SGS scalar FDFs in these contributions are based on the first and the second order moments. The PDFs generated in this way facilitate affordable LES. However, it now is well understood that the true PDF depends strongly on the actual physics of mixing in a given flow condition [35].

1.1 Our Previous Work in LES/FDF

A reliable means of determining the FDF is via solution of its transport equation. A systematic study in this endeavor was initiated by Colucci *et al.* [10], who developed and solved a modelled transport equation for the marginal scalar FDF (SFDF) in constant density reacting flows. This work demonstrated, for the first time, the feasibility of LES/FDF and the importance of SGS scalar fluctuation for accurate modeling of the filtered reaction rate. The extension of this work was conducted by Jaberi *et al.* [34, 36], who developed the marginal scalar filtered mass density function (SFMDF). The SFMDF is essentially the mass-weighted form of the SFDF. Due to the marginal nature of the FDFs in these studies, all of the hydrodynamic effects, including all of the velocity-scalar correlations, are modelled via conventional

(non-FDF) methods. The extension for modeling of the velocity field was done by Gicquel *et al.* [23], who developed and solved a transport equation for the marginal velocity FDF (VFDF) in constant density flows. This work demonstrated some of the advantages of the FDF in comparison to conventional methods in accounting for the effects of SGS velocity correlations.

1.2 Related Work by Others

Since its original conception [24, 65], the FDF has become very popular for combustion applications. In addition to our previous work, as cited above, the methodology has experienced widespread usage by many others. Examples are contributions in its basic implementations [90, 26, 70], fine-tuning of its sub-closures [72, 8, 31], and its validation via laboratory experiments [82, 86, 83, 87]. The methodology is finding its way into commercial codes [26, 9] and has been the subject of detailed discussions in several recent textbooks [67, 19, 32].

2 Accomplishments

The goal of this research was to improve the capabilities of the FDF method and to implement it for LES of chemically reacting turbulent flows. We feel that we have been very successful in achieving the specific objectives of this work. These objectives were:

1. development and implementation of the joint velocity-scalar filtered density function (VSFDF) for SGS modeling of turbulent combustion,
2. fine-tuning and implementation of the scalar FDF (SFDF) for LES of complex flames and comparison with experimental data.

The efforts pertaining to these objectives are described partly in Refs. [79] and [78] and discussed further below. In addition, the PI has provided an invited survey article [25] with a review of FDF methods. The discussions provide a comprehensive description of our accomplishments but do not emphasize the materials published in articles [79] and [78].

2.1 Fundamental Formulation

In a compressible flow undergoing chemical reaction involving N_s species, the primary transport variables are the density $\rho(\mathbf{x},t)$, the velocity vector $u_i(\mathbf{x},t)$ $(i=1,2,3)$, the pressure $p(\mathbf{x},t)$, the total specific enthalpy $h(\mathbf{x},t)$ and the species' mass fractions $Y_\alpha(\mathbf{x},t)$ $(\alpha=1,2,\ldots,N_s)$. The equations that describe the transport of these variables in space (x_i) $(i=1,2,3)$ and time (t) are the continuity, momentum, enthalpy (energy), and species' mass fraction equations, along with an equation of state

$$\frac{\partial \rho}{\partial t}+\frac{\partial \rho u_j}{\partial x_j} = 0, \tag{1a}$$

$$\frac{\partial \rho u_i}{\partial t}+\frac{\partial \rho u_j u_i}{\partial x_j} = -\frac{\partial p}{\partial x_i}+\frac{\partial \tau_{ji}}{\partial x_j}, \tag{1b}$$

$$\frac{\partial \rho \phi_\alpha}{\partial t}+\frac{\partial \rho u_j \phi_\alpha}{\partial x_j} = -\frac{\partial J_j^\alpha}{\partial x_j}+\rho S_\alpha, \quad \alpha=1,2,\ldots,\sigma=N_s+1, \tag{1c}$$

$$p = \rho R_0 T\sum_{\alpha=1}^{N_s} Y_\alpha/M_\alpha = \rho R T, \tag{1d}$$

where R_0 and R are the universal and mixture gas constants and M_α denotes the molecular weight of species α. The chemical reaction source terms $S_\alpha \equiv S_\alpha(\boldsymbol{\phi}(\mathbf{x},t))$ are functions of compositional scalars $(\boldsymbol{\phi} \equiv [\phi_1,\phi_2,\ldots,\phi_{N_s+1}])$. Equation (1c) represents the transport of species' mass fraction and enthalpy in a common form with

$$\phi_\alpha \equiv Y_\alpha, \quad \alpha=1,2,...,N_s, \qquad \phi_\sigma \equiv h=\sum_{\alpha=1}^{N_s} h_\alpha \phi_\alpha, \tag{2}$$

and

$$h_\alpha = h_\alpha^0+\int_{T_0}^{T} c_{p_\alpha}(T')dT'. \tag{3}$$

Here T and T_0 denote the temperature field and the reference temperature, respectively. In this equation, h_α^0 and c_{p_α} denote the absolute enthalpy at T_0 and the specific heat at constant pressure for species α. For a Newtonian fluid, with Fick's law of diffusion, the viscous stress tensor τ_{ij} and the scalar flux J_j^α are represented by

$$\tau_{ij} = \mu\left(\frac{\partial u_i}{\partial x_j}+\frac{\partial u_j}{\partial x_i}-\frac{2}{3}\frac{\partial u_k}{\partial x_k}\delta_{ij}\right), \tag{4a}$$

$$J_j^\alpha = -\gamma\frac{\partial \phi_\alpha}{\partial x_j}, \tag{4b}$$

where μ is the fluid dynamic viscosity and $\gamma = \rho\Gamma$ denote the thermal and mass molecular diffusivity coefficients for all scalars. In reactive flows, molecular processes are much more complicated than portrayed by Eq. (4). Since the molecular diffusion typically is less important than that of SGS turbulence, this simple model is adopted with the justifications and caveats given in Refs. [44, 64] and [3].

Large eddy simulation involves the spatial filtering operation [67, 63, 52, 22, 75]

$$\langle Q(\mathbf{x},t)\rangle_\ell = \int_{-\infty}^{+\infty} Q(\mathbf{x}',t)G(\mathbf{x}',\mathbf{x})d\mathbf{x}', \tag{5}$$

where $G(\mathbf{x}',\mathbf{x})$ denotes a filter function, and $\langle Q(\mathbf{x},t)\rangle_\ell$ is the filtered value of the transport variable $Q(\mathbf{x},t)$. In variable-density flows it is convenient to use the Favré-filtered quantity $\langle Q(\mathbf{x},t)\rangle_L = \langle \rho Q\rangle_\ell / \langle\rho\rangle_\ell$. We consider a filter function that is spatially and temporally invariant and localized. Thus, $G(\mathbf{x}',\mathbf{x}) \equiv G(\mathbf{x}'-\mathbf{x})$ with the properties $G(\mathbf{x}) \geq 0$, $\int_{-\infty}^{+\infty} G(\mathbf{x})d\mathbf{x} = 1$. Applying the filtering operation to Eqs. (1) and using the conventional LES approximation for the diffusion terms, we obtain

$$\begin{aligned}\frac{\partial \langle\rho\rangle_\ell \langle u_i\rangle_L}{\partial t} + \frac{\partial \langle\rho\rangle_\ell \langle u_j\rangle_L \langle u_i\rangle_L}{\partial x_j} &= -\frac{\partial \langle p\rangle_\ell}{\partial x_i} + \frac{\partial}{\partial x_j}\left[\mu\left(\frac{\partial \langle u_i\rangle_L}{\partial x_j} + \frac{\partial \langle u_j\rangle_L}{\partial x_i}\right)\right] \\ &\quad - \frac{2}{3}\frac{\partial}{\partial x_i}\left(\mu\frac{\partial \langle u_j\rangle_L}{\partial x_j}\right) - \frac{\partial \langle\rho\rangle_\ell \tau_L(u_i,u_j)}{\partial x_j}, \qquad (6a)\\ \frac{\partial \langle\rho\rangle_\ell \langle\phi_\alpha\rangle_L}{\partial t} + \frac{\partial \langle\rho\rangle_\ell \langle u_j\rangle_L \langle\phi_\alpha\rangle_L}{\partial x_j} &= \frac{\partial}{\partial x_j}\left(\gamma\frac{\partial \langle\phi_\alpha\rangle_L}{\partial x_j}\right) - \frac{\partial \langle\rho\rangle_\ell \tau_L(u_j,\phi_\alpha)}{\partial x_j} + \langle\rho S_\alpha\rangle_\ell, \qquad (6b)\end{aligned}$$

where

$$\tau_L(a,b) = \langle ab\rangle_L - \langle a\rangle_L \langle b\rangle_L \tag{7}$$

The "velocity-scalar filtered mass density function" (VSFMDF), denoted by $F_L(\boldsymbol{v},\boldsymbol{\psi};\mathbf{x},t)$, is defined formally as [65]

$$F_L(\boldsymbol{v},\boldsymbol{\psi};\mathbf{x},t) = \int_{-\infty}^{+\infty} \rho(\mathbf{x}',t)\zeta\left(\boldsymbol{v},\boldsymbol{\psi};\boldsymbol{u}(\mathbf{x}',t),\boldsymbol{\phi}(\mathbf{x}',t)\right)G(\mathbf{x}'-\mathbf{x})d\mathbf{x}', \tag{8}$$

where

$$\zeta\left(\boldsymbol{v},\boldsymbol{\psi};\boldsymbol{u}(\mathbf{x},t),\boldsymbol{\phi}(\mathbf{x},t)\right) = \prod_{i=1}^{3}\delta\left(v_i - u_i(\mathbf{x},t)\right) \times \prod_{\alpha=1}^{\sigma}\delta\left(\psi_\alpha - \phi_\alpha(\mathbf{x},t)\right). \tag{9}$$

In this equation, δ denotes the Dirac delta function, and $\boldsymbol{v},\boldsymbol{\psi}$ are the velocity vector

and the scalar array in the sample space. The term ζ is the "fine-grained" density [60, 64]. Equation (8) defines the velocity-scalar filtered mass density function (VSFMDF) as the spatially filtered value of the fine-grained density. With the condition of a positive filter kernel [84], F_L has all of the properties of a mass density function [64]. For further developments it is useful to define the "conditional filtered value" of the variable $Q(\mathbf{x},t)$ as

$$\left\langle Q(\mathbf{x},t) \,\middle|\, \boldsymbol{u}(\mathbf{x},t)=\boldsymbol{v}, \boldsymbol{\phi}(\mathbf{x},t)=\boldsymbol{\psi} \right\rangle_\ell \equiv \left\langle Q \,\middle|\, \boldsymbol{v},\boldsymbol{\psi} \right\rangle_\ell = \frac{\int_{-\infty}^{+\infty} Q\left(\mathbf{x}',t\right)\rho(\mathbf{x}',t)\zeta\left(\boldsymbol{v},\boldsymbol{\psi};\boldsymbol{u}(\mathbf{x}',t),\boldsymbol{\phi}(\mathbf{x}',t)\right)G\left(\mathbf{x}'-\mathbf{x}\right)d\mathbf{x}'}{F_L\left(\boldsymbol{v},\boldsymbol{\psi};\mathbf{x},t\right)}. \tag{10}$$

To develop the VSFMDF transport equation, we consider the time derivative of the fine-grained density function, (Eq. (9)). Filtering of this equation yields [77]

$$\begin{aligned}
\frac{\partial F_L}{\partial t}+\frac{\partial v_i F_L}{\partial x_i} &= -\frac{\partial}{\partial \psi_\alpha}\left[S_\alpha(\boldsymbol{\psi})F_L\right] \\
&+ \frac{\partial}{\partial v_i}\left(\left\langle \frac{1}{\rho(\boldsymbol{\phi})}\frac{\partial p}{\partial x_i}\,\middle|\, \boldsymbol{v},\boldsymbol{\psi}\right\rangle_\ell F_L\right) \\
&- \frac{\partial}{\partial v_i}\left(\left\langle \frac{1}{\rho(\boldsymbol{\phi})}\frac{\partial \tau_{ji}}{\partial x_j}\,\middle|\, \boldsymbol{v},\boldsymbol{\psi}\right\rangle_\ell F_L\right) \\
&+ \frac{\partial}{\partial \psi_\alpha}\left(\left\langle \frac{1}{\rho(\boldsymbol{\phi})}\frac{\partial J_i^\alpha}{\partial x_i}\,\middle|\, \boldsymbol{v},\boldsymbol{\psi}\right\rangle_\ell F_L\right),
\end{aligned} \tag{11}$$

which is an exact transport equation and indicates that the effects of convection (second term on LHS) and chemical reaction (the first term on RHS) appear in closed form. The unclosed terms denote convective effects in the velocity-scalar sample space. Integrating this equation over the $\boldsymbol{v}$ field yields the transport equation for the scalar filtered mass density function (SFMDF) $F_L(\boldsymbol{\psi};\mathbf{x},t)$,

$$\begin{aligned}
\frac{\partial F_L(\boldsymbol{\psi};\mathbf{x},t)}{\partial t}+\frac{\partial[\langle u_i(\mathbf{x},t)|\boldsymbol{\psi}\rangle_\ell F_L(\boldsymbol{\psi};\mathbf{x},t)]}{\partial x_i} &= -\frac{\partial}{\partial \psi_\alpha}[S_\alpha(\boldsymbol{\psi})F_L(\boldsymbol{\psi};\mathbf{x},t)] \\
&+ \frac{\partial}{\partial \psi_\alpha}\left[\left\langle \frac{1}{\rho(\boldsymbol{\phi})}\frac{\partial J_i^\alpha}{\partial x_i}\,\middle|\, \boldsymbol{\psi}\right\rangle_\ell F_L(\boldsymbol{\psi};\mathbf{x},t)\right]
\end{aligned} \tag{12}$$

which is an exact transport equation for the SFMDF. The first term on the right hand-side of this equation is due to chemical reaction and is in closed form. The unclosed nature of SGS convection and mixing is indicated by the conditional filtered values.

For closure of the VSFMDF transport equation, following previous work [28, 17, 10, 23, 79], we utilize the generalized Langevin model (GLM) and the linear mean square estimation (LMSE) model [60]. We assume a constant value for $\mu = \gamma$; *i.e.* unity Schmidt (Sc) and Lewis (Le) numbers. With these assumptions, the model is:

$$
\begin{aligned}
\mathrm{dX}_i^+ &= U_i^+ \, dt + \sqrt{\frac{2\mu}{\langle\rho\rangle_\ell}} \, dW_i, && \text{(13a)} \\
dU_i^+ &= \left[-\frac{1}{\langle\rho\rangle_\ell} \frac{\partial \langle p \rangle_l}{\partial x_i} + \frac{2\mu}{\langle\rho\rangle_\ell} \frac{\partial^2 \langle u_i \rangle_L}{\partial x_j \partial x_j} + \frac{\mu}{\langle\rho\rangle_\ell} \frac{\partial^2 \langle u_j \rangle_L}{\partial x_j \partial x_i} - \frac{2}{3} \frac{\mu}{\langle\rho\rangle_\ell} \frac{\partial^2 \langle u_j \rangle_L}{\partial x_i \partial x_j} \right] dt \\
&+ G_{ij} \left(U_j^+ - \langle u_j \rangle_L \right) dt + \sqrt{C_0 \epsilon} \, dW_i' + \sqrt{\frac{2\mu}{\langle\rho\rangle_\ell}} \frac{\partial \langle u_i \rangle_L}{\partial x_j} \, dW_j, && \text{(13b)} \\
d\phi_\alpha^+ &= -C_\phi \omega \left(\phi_\alpha^+ - \langle \phi_\alpha \rangle_L \right) dt + S_\alpha(\boldsymbol{\phi}^+) \, dt, && \text{(13c)}
\end{aligned}
$$

where $X_i^+, U_i^+, \phi_\alpha^+$ are probabilistic representations of position, velocity vector, and scalar variables, respectively. Also:

$$
\begin{aligned}
G_{ij} &= -\omega \left(\frac{1}{2} + \frac{3}{4} C_0 \right) \delta_{ij} \\
\omega &= \frac{\epsilon}{k} \\
\epsilon &= C_\epsilon \frac{k^{3/2}}{\Delta_L} \\
k &= \frac{1}{2} \tau_L \left(u_k, u_k \right). && \text{(14)}
\end{aligned}
$$

Here ω is the SGS mixing frequency, ϵ is the SGS dissipation rate, k is the SGS kinetic energy, and Δ_L is the LES filter size. The parameters C_0, C_ϕ and C_ϵ are model constants and need to be specified. Thus, the Fokker-Planck equation [74] is:

$$
\begin{aligned}
\frac{\partial F_L}{\partial t}+\frac{\partial v_i F_L}{\partial x_i} &= \frac{1}{\langle\rho\rangle_l}\frac{\partial\langle p\rangle_l}{\partial x_i}\frac{\partial F_L}{\partial v_i}-\frac{2\mu}{\langle\rho\rangle_l}\frac{\partial^2\langle u_i\rangle_L}{\partial x_j\partial x_j}\frac{\partial F_L}{\partial v_i}-\frac{\mu}{\langle\rho\rangle_l}\frac{\partial^2\langle u_j\rangle_L}{\partial x_i\partial x_j}\frac{\partial F_L}{\partial v_i}\\
&+ \frac{2}{3}\frac{\mu}{\langle\rho\rangle_l}\frac{\partial^2\langle u_j\rangle_L}{\partial x_j\partial x_i}\frac{\partial F_L}{\partial v_i}-G_{ij}\frac{\partial\left[\left(v_j-\langle u_j\rangle_L\right)F_L\right]}{\partial v_i}+\mu\frac{\partial^2\left(F_L/\langle\rho\rangle_l\right)}{\partial x_j\partial x_j}\\
&+ \frac{\partial}{\partial x_j}\left(\frac{2\mu}{\langle\rho\rangle_l}\frac{\partial\langle u_i\rangle_L}{\partial x_j}\frac{\partial F_L}{\partial v_i}\right)+\frac{\mu}{\langle\rho\rangle_l}\frac{\partial\langle u_i\rangle_L}{\partial x_k}\frac{\partial\langle u_j\rangle_L}{\partial x_k}\frac{\partial^2 F_L}{\partial v_i\partial v_j}+\frac{1}{2}C_0\epsilon\frac{\partial^2 F_L}{\partial v_j\partial v_j}\\
&+ C_\phi\omega\frac{\partial\left[\left(\psi_\alpha-\langle\phi_\alpha\rangle_L\right)F_L\right]}{\partial\psi_\alpha}-\frac{\partial\left[S_\alpha(\boldsymbol{\psi})F_L\right]}{\partial\psi_\alpha}. \qquad (15)
\end{aligned}
$$

The transport equations for the filtered variables are obtained by integration of Eq. (15). For the marginal SFMDF, the model for the scalar transport is the same. But the velocity field must be obtained by other (non-FDF) means. In this case, the physical transport is modelled via:

$$
dX_i(t)=\left[\langle u_i\rangle_L+\frac{1}{\langle\rho\rangle_\ell}\frac{\partial(\gamma+\gamma_t)}{\partial x_i}\right]dt+\sqrt{2(\gamma+\gamma_t)/\langle\rho\rangle_\ell}dW_i(t) \qquad (16)
$$

which yields the modelled transport equation for the SFMDF:

$$
\frac{\partial F_L}{\partial t}+\frac{\partial[\langle u_i\rangle_L F_L]}{\partial x_i}=\frac{\partial}{\partial x_i}\left[(\gamma+\gamma_t)\frac{\partial(F_L/\langle\rho\rangle_\ell)}{\partial x_i}\right]+\frac{\partial}{\partial\psi_\alpha}\left[\Omega_m(\psi_\alpha-\langle\phi_\alpha\rangle_L)F_L\right]-\frac{\partial[S_\alpha F_L]}{\partial\psi_\alpha}. \qquad (17)
$$

Here, γ_t is the SGS diffusivity and must be modelled. The modified kinetic energy viscosity (MKEV) model of Jaberi *et al.* [34] has proven effective for this purpose. The model in this way is equivalent of the gradient-diffusion model for the SGS flux of the scalars:

$$
\langle\rho\rangle_\ell\tau_L(u_j,\phi_\alpha)=-\gamma_t\frac{\partial\langle\phi_\alpha\rangle_L}{\partial x_j} \qquad (18)
$$

The mixing frequency here is denoted by Ω_m to distinguish it from that in the VSFMDF because it has to be modelled differently. The model proposed by Colucci *et al.* [10]

$$
\Omega_m=\frac{C_\phi(\gamma+\gamma_t)}{\langle\rho\rangle_\ell\Delta_L^2} \qquad (19)
$$

has been used in almost all of the previous applications of SFMDF.

From the computational standpoint, solution of the SDEs (*e.g.* Eq. (13) and/or Eq. (16) is significantly easier than the modelled FDF transport equations (15), (17). The most effective way of solving Eq. (13) and/or Eq. (16)) is via Monte Carlo

(MC) methods. These methods have been used for simulation of a wide variety of stochastic problems [27] and have benefitted significantly from modern developments in SDE solver technology [42]. MC methods have been the primary means of solving the PDF in RAS [64, 29, 30, 66, 89] and, thus far, the primary method of choice for solving the FDF in LES. Typically, the method is implemented by representing the FDF by an ensemble of, say N_p, particles. These particles carry information pertaining to their positions, $\mathbf{X}^{(n)}(t)$, velocities, $\mathbf{U}^{(n)}(t)$, and scalar values, $\boldsymbol{\phi}^{(n)}(t)$, $n = 1, \ldots, N_p$. This information is updated via temporal integration of the modelled SDEs. While it is potentially, or eventually, possible to simulate FDF exclusively via MC, the most practical procedure is via "hybrid" methods in conjunction with "deterministic" schemes. There has been significant progress in the development of high-order finite difference (FD), finite volume, and spectral methods. A hybrid method would make use of this high-order accuracy which is not yet achievable in methods exclusively via MC. Moreover, the influence of the MC dispersion and statistical errors is less significant in hybrid methods. Finally, in many cases it is easier to specify the model parameters in a deterministic fashion than via MC. These issues are investigated in detail in the context of RAS/PDF [57, 59] and constitute a major element of the computational procedure in LES/FDF [34, 23, 79].

The base flow simulations are based on a compact parameter finite-difference (FD) scheme [7, 41] on a number of fixed grid points with spatial spacing Δ. The MC particles are distributed randomly and are free to move anywhere within the domain. The statistical information, *e.g.* filtered values, at any point is obtained by considering an ensemble of N_E particles residing within an ensemble domain of side length Δ_E centered around the points. For reliable statistics with minimal numerical dispersion, it is desired to minimize the size of ensemble domain and maximize the number of the MC particles [64]. In this way, the ensemble statistics would tend to the desired filtered values. Transfer of information from the grid points to the MC particles is accomplished via interpolation. The transfer of information from the particles to the grid points is accomplished via ensemble averaging as described above.

The FD solver determines the pressure field which is used further in the MC procedure. The transport equations solved by the FD include unclosed second order moments which are obtained from the MC solver. The FD solver also determines the filtered velocity and scalar fields. That is, there is a "redundancy" in the determination of the first filtered moments as both the FD and the MC procedures provides the solution of this field. This redundancy actually is very useful in monitoring the accuracy of the simulated results as shown in previous

work [34, 57, 59, 23, 79].

To reduce the computational cost, a procedure involving the use of non-uniform weights [34] also is considered. This procedure allows a smaller number of particles in regions where a low degree of variability is expected. Conversely, in regions of high variability, a large number of particles is allowed. It has been shown [64, 34] that the sum of weights within the ensemble domain is related to filtered fluid density, and the Favré-filtered values are constructed from the weighted average values. With uniform weights [64], the particle number density decreases significantly in regions of low density, such as reaction zone. The implementation of variable weight allows the increase in particle density without increasing the particle number density in these regions.

2.2 Latest Results via VSFMDF

Simulations are conducted of a three-dimensional temporally developing mixing layer involving transport of a passive scalar. The VSFMDF predictions are compared with data obtained by direct numerical simulation (DNS) of the same flow. For a comparative assessment against a conventional method, LES of this layer also is performed using the Smagorinsky [80] SGS closure. In the representation below, x, y, and z denote the streamwise, the cross-stream, and the spanwise directions, respectively. The velocity components along these directions are denoted by u, v, and w in the x, y, and z directions, respectively. The temporal mixing layer consists of two parallel streams travelling in opposite directions with the same speed [73, 76, 56]. The normalized filtered streamwise velocity, scalar, and temperature fields are initialized with hyperbolic tangent profiles with $\langle u \rangle_L = 1$, $\langle \phi \rangle_L = 1$, $\langle T \rangle_L = 1$ for the top stream and $\langle u \rangle_L = -1$, $\langle \phi \rangle_L = 0$, $\langle T \rangle_L = 2$ for the bottom stream. The length L_v is specified such that $L_v = 2^{N_P} \lambda_u$, where N_P is the desired number of successive vortex pairings and λ_u is the wavelength of the most unstable mode corresponding to the mean streamwise velocity profile imposed at the initial time. The flow variables are normalized with respect to the half initial vorticity thickness, $L_r = \frac{\delta_v(t=0)}{2}$, ($\delta_v = \frac{\Delta U}{|\partial \overline{\langle u \rangle_L} / \partial y|_{max}}$, where $\overline{\langle u \rangle_L}$ is the Reynolds-averaged value of the filtered streamwise velocity and ΔU is the velocity difference across the layer).

We consider a cubic box, $0 \leq x \leq L$, $\frac{-L}{2} \leq y \leq \frac{L}{2}$, $0 \leq z \leq L$ where $L = L_v / L_r$. The 3D field is parameterized in a procedure somewhat similar to that in Ref. [85]. Simulations are conducted on equal grid spacings $\Delta x = \Delta y = \Delta z = \Delta$ with the

number of grid points 193^3 and 33^3 for DNS and LES, respectively. The number of particles per grid point is $NPG = 320$ ($N_E = 40$) and the ensemble domain size is set equal to $\Delta_E \times \Delta_E \times \Delta_E$ where $\Delta_E = \Delta/2$. For comparison, the DNS data are filtered from the original high resolution to the coarse points using a top-hat filter function with the filter size (Δ_L) equal to 2Δ.

The formation of the large scale structures are expedited through eigenfunctions based initial perturbations [53, 45]. We impose two-dimensional [76, 85, 54] and three-dimensional [76, 55] perturbations with a random phase shift between the $3D$ modes. This forcing results in the formation of two successive vortex pairings and strong three-dimensionality. For a statistical appraisal, we also consider the "resolved" and the "total" components of the Reynolds-averaged moments. The former are denoted by $\overline{R(a,b)}$ with $R(a,b) = \left(\langle a\rangle_L - \overline{\langle a\rangle_L}\right)\left(\langle b\rangle_L - \overline{\langle b\rangle_L}\right)$; and the latter are $\overline{r(a,b)}$ with $r(a,b) = (a-\overline{a})\left(b-\overline{b}\right)$. In DNS, the "total" components are available directly, while in LES they are approximated by $\overline{r(a,b)} \approx \overline{R(a,b)} + \overline{\tau_L(a,b)}$ [85].

Figure 1 shows the instantaneous iso-surface of the $\langle\phi\rangle_L$ field at $t = 80$ as obtained by DNS and by VSFMDF and Smagorinsky models. By this time, the flow is going through pairings and exhibits strong 3D effects [53]. The two neighboring rollers are being paired, and the formation of secondary structures is evident. As illustrated in this figure and consistent with the previous results [23], the amount of SGS diffusion with the Smagorinsky model is significant. Thus, the predicted results are overly smooth, while there is more resemblance between the VSFMDF and DNS results.

Several components of the Reynolds-averaged values of the second order SGS moments are compared with DNS data in Fig. 2. In general, the VSFMDF results are in better agreement with DNS data than those predicted by the Smagorinsky model. In this configuration, there are no strong velocity and scalar gradients in the streamwise and spanwise directions, and, thus, a gradient-diffusion type model such as Smagorinsky is not capable of providing correct prediction of scalar flux values in these directions. Consequently, the VSFMDF is expected to be more effective for LES of reacting flows, provided that the extent of SGS mixing is influenced heavily by these SGS moments [4, 62]. Several components of the resolved second order moments are presented in Fig. 3. As expected, the performance of the Smagorinsky model is not satisfactory, as it does not predict the spread and peak values accurately. The VSFMDF provides more reasonable predictions. The "total" components also yield very good agreement with DNS data, as shown in Fig. 4. As observed in Refs. [79, 23], the "total" components predicted by VSFMDF are almost insensitive to

the model parameters.

2.3 Latest Results via SFMDF

LES via SFMDF was conducted of a turbulent bluff-body stabilized hydrogen-methane jet flame. This flame has been studied experimentally by the Combustion Research Facility at the Sandia National Laboratories and the Thermal Research Group at the University of Sydney [49, 48, 50, 14, 13, 12, 2, 1]. Bluff-body stabilized flames have been studied by several investigators [51, 38, 58, 46, 68, 69, 70, 33, 88, 43, 12]. These flames produce complex flow patterns characteristic of practical combustors, and are important for industrial applications.

In the experiments, a variety of operating conditions are considered. The flow schematic is shown in Fig. 5. The central round fuel jet is surrounded by a round bluff-body and air coflow. The jet diameter D_J=3.6 mm, and the bluff-body diameter D_B=50 mm. The recirculation zone immediately follows the bluff-body surface. The neck zone provides a controlled region where the turbulent mixing rate is significant and flame blow-off (extinction) can occur [12]. Further downstream, the flame exhibits jet like behavior. Both non-reacting and reacting flows are considered. The experiments pertaining to the former are distinguished by their corresponding bulk jet velocities, U_J, while those of the latter are distinguished by their blow-off parameter. The recirculation zones differ in length from $\sim 1.0D_B$ for the non-reacting cases to $\sim 1.6D_B$ for the reacting cases. The reacting case is characterized by a Reynolds number of 15,800 based on fuel jet diameter and bulk jet velocity. The bulk jet and the coflow velocities are 118 m/s and 40 m/s, respectively. This condition corresponds to 50% blow-off. The 100% blow-off velocity of the flame is U_{BO}=235 m/s.

The most complete set of measurements has been compiled for the hydrogen-methane flames. These flames are considered at 50%, 75%, and 91% blow-off (extinction). The jet is maintained at a temperature of 298 K and is composed of 50% hydrogen (H_2) and 50% methane (CH_4) by volume [13]. The dilution of hydrogen in methane reduces the formation of soot. The coflow is maintained at room temperature and is composed of air. The bluff-body is a ceramic surface that heated up to an average of 1003 K during operation. The effects of radiative heat transfer on the temperature and other major species are small [33].

LES is conducted of the 50% blow-off case. The chemistry is near-equilibrium and is parameterized by the flamelet library constructed by simulation of a counterflow

(opposed jet) laminar flame [61]. This flame is modelled with detailed chemical kinetics [81, 6]. At low strain rates, χ, all of the thermo-chemical variables are related to the "mixture fraction" $Z(\mathbf{x},t)$; that is, $Q(\mathbf{x},t) \equiv \hat{Q}(Z(\mathbf{x},t))$. Therefore, $\langle\rho(\mathbf{x},t)\rangle_\ell \langle Q(\mathbf{x},t)\rangle_L = \int_{-\infty}^{+\infty} \hat{Q}(\psi_Z) F_L(\psi_Z;\mathbf{x},t)\, d\psi_Z$. The flamelet table constructed in this way is used in conjunction with SFMDF predictions of the mixture fraction.

The simulations are conducted on a 3D Cartesian mesh with uniformly spaced grid points. The computational domain spans a region of $30D_J \times 22.5D_J \times 22.5D_J$ in the streamwise (x), and the two lateral (y, z) directions, respectively. The number of grid points is $101 \times 151 \times 151$ in the x, y, and z directions, respectively. The filter size is set at $\Delta_L = 2(\Delta x \Delta y \Delta z)^{1/3}$, where the Δx, Δy, and Δz are the grid spacings in the corresponding directions. The size of the ensemble domain in the MC simulation is equal to the filter size. There are approximately 40 particles in each ensemble domain. Per results of extensive previous studies [34, 10, 23, 79], this number is sufficient to yield an excellent statistical accuracy, with minimal dispersive errors. There are about 6.8 million MC particles within the computational domain at all times. The results are monitored to ensure that the particles fully encompass and extend well beyond the regions of non-zero vorticity and reaction.

The statistics are obtained by long-time averaging of the Favré filtered fields during several residence times. Data collection is initialized after the flow has swept the domain during the initial four flow through times. The PDFs are constructed based on the SFMDF data resolved at the FD grid points. The notations $\overline{Q}$ and $RMS(Q)$ denote the time-averaged mean and root mean square values of the variable Q, respectively. The radial direction is denoted by $r = \sqrt{y^2 + z^2}$. The flamelet table with a constant strain rate of $\chi = 100\ 1/s$ is used. This choice is consistent with previous studies of bluff-body flames [58] and experimental assessments [13].

Tables 1 and 2 show the specifications of the experiments and simulation data, respectively. The experimental flow fields of the reacting cases HM1E-S(1-2) considered at Sydney are meant to represent the same flame conditions as the HM1 experiments considered at Sandia. However, the wind tunnel in Sydney did not provide the same hydrodynamic conditions. The streamwise velocities are $U_J = 118m/s$ and $U_C = 40m/s$ in the HM1, and $U_J = 108m/s$ and $U_C = 35m/s$ in the HM1E-S experiments. The new jet and coflow velocities were chosen such that the HM1 and HM1E-S flames are equally proportional (within 50% blow-off) to their corresponding blow-off velocities. To facilitate comparisons of the flow statistics of the HM1E-S data with those of HM1 and SFMDF, the HM1E-S values of the streamwise velocity are scaled by a ratio of the bulk jet velocities; that is 118/108.

Table 1: Experimental specifications [1].

Label	Fuel(Ratio†)	U_J‡	U_{CO}[c]	Available data	Year
B4C1-S1	Air	61	20	$\overline{U}$, $\overline{V}$, $RMS(U)$, $RMS(V)$	1995
B4C1-S2	Air	61	20	$\overline{U}$, $\overline{V}$, $RMS(U)$, $RMS(V)$, $RMS(UV)$	12/01/1999
B4C1-S3	Air	61	20	$\overline{U}$, $\overline{V}$, $RMS(U)$ $RMS(V)$, $RMS(UV)$	12/15/1999
B4C2-50	CNG	50	20	$\overline{Z}$, $RMS(Z)$	
B4C2-85	CNG	85	20	$\overline{Z}$, $RMS(Z)$	
B4C2-143	CNG	143	20	$\overline{Z}$, $RMS(Z)$	
HM1	$H_2 : CNG$ $(1:1)$	118	40	$\overline{U}$, $\overline{V}$, $RMS(U)$, $RMS(V)$	1995
HM1	$H_2 : CH_4$ $(1:1)$	118	40	$\overline{Z}$, $\overline{T}$, $\overline{Y_\alpha}$§, $RMS(Z)$, $RMS(T)$, $RMS(Y_\alpha)$, PDFs	1995
HM1E-S1	$H_2 : CNG$ $(1:1)$	108	35	$\overline{U}$, $\overline{V}$, $RMS(U)$, $RMS(V)$, $RMS(UV)$	01/21/2000
HM1E-S2	$H_2 : CNG$ $(1:1)$	108	35	$\overline{U}$, $\overline{V}$, $RMS(U)$, $RMS(V)$, $RMS(UV)$	02/11/2000

†Volumetric.
‡[m/s]
§O_2, N_2, H_2, H_2O, CO, CO_2, OH, NO

Table 2: Simulation specifications.

Label	Fuel(Ratio†)	U_J‡	U_{CO}[c]	Re§
LES-61	Air	61	20	13899
LES-50	CH_4	50	20	10580
LES-85	CH_4	85	20	17987
LES-143	CH_4	143	20	30260
SFMDF	$H_2 : CH_4$ $(1:1)$	118	40	15800

†Volumetric.
‡[m/s]
§Reynolds number based on D_J and U_J

The non-reacting experiments, B4C1-S(1-3), consider air at both the fuel and coflow streams. The bulk streamwise velocity of 61 m/s and the coflow streamwise velocity of 20 m/s are considered. The recirculation zone with the double vortex structures captured by the experiments and LES are shown via the time-averaged streamwise velocity contours with superimposed streamlines and velocity vectors in Fig. 6. The model captures the two recirculation zones well. The length of the recirculation region behind the bluff-body surface is overpredicted slightly. The counter-rotating vortices also are predicted slightly further downstream from their experimentally reported counterparts.

The non-reacting experiments, B4C2, consider a "cold" methane fuel stream with bulk streamwise velocities of 50, 85, and 143 m/s, and the air coflow stream with the streamwise velocity of 20 m/s. The time averaged streamwise velocity with superimposed streamlines and velocity vectors are shown in Fig. 7. As observed previously, a set of two counter-rotating vortices forms behind the bluff-body surface. The recirculation region shortens as the fuel stream velocity increases. In addition, the two vortices reposition themselves, with the inner vortex shifting downstream with respect to the outer one. The shift is accompanied by a loss in inner vortex circulation strength that becomes most noticeable in LES-143. In the latter case large streamwise velocity causes the inner vortex to break down partially. The instantaneous and the time-averaged 3D contours of the mixture fraction are shown in Fig. 8. Different mixing structures are observed in the instantaneous values as the streamwise velocity of the fuel stream increases. The time-averaged plots accentuate the shortening of the recirculation zone as highlighted by the "cone" of the mixture fraction iso-surface of 0.06.

The capability of the SFMDF to predict the reacting flow field now is demonstrated. The time averaged streamwise velocity contours with the streamlines and velocity vectors superimposed are shown in Fig. 9. This figure shows the recirculation region and the two characteristic counter-rotating vortices. The recirculating zones are captured well by the simulations. However, there are a few discrepancies that are manifested by the relative position of the inner and outer vortices. In the HM1 experiment, as well as in the simulation, the inner vortex is located behind the outer vortex. However, in the HM1E-S experiments the situation is reversed. The recirculating region extends to $\sim 1.6D_B$, as compared to $\sim 1D_B$ in the isothermal cases. The central jet penetrates more easily the low density region. The mean profiles of the streamwise velocity and the mixture fraction are shown in Figs. 10 and 11, respectively. The comparisons show good overall qualitative agreement with data.

The radial profiles of the mean and the RMS values of the temperature are shown in Figs. 12 and 13, respectively. The near field mean values compare well with the experimental data. The downstream locations, however, are overpredicted on the oxidizer stream side of the bluff-body. The overprediction can be traced to the temperature on the fuel lean side of the flamelet table. The mean temperature is the highest in the central mixing layer region where the hot products of combustion are convected toward the bluff-body by the counter-rotating vortical structures. The experimental temperature RMS values are overpredicted by the total RMS values and generally are predicted well by the resolved RMS values with the exception of the oxidizer stream side of the bluff-body at downstream locations. Similar to the mixture fraction RMS, the effects of the three mixing layers, generated by the counter-rotating vortical structures, are characterized at $x/D_B = 0.8$ and $r/R_B \approx 0.2,\ 0.5,\ 0.9$ by the peaking RMS values of the temperature. The PDFs of the resolved scalar fields, as predicted by SFMDF, are compared with those measured experimentally in Fig. 14 for the resolved mixture fraction and Fig. 15 for the resolved temperature. The overall agreement between SFMDF predictions and the experiment is very good.

2.4 Computational Requirements

For the computational requirements of FDF, the relative, normalized run times for conventional (non-FDF): SFDF : VSFDF : DNS are: (1) : $(3-5)$: $(15-20)$: $(1500-2000)$. Obviously, the most serious issue associated with FDF is its computational cost. In most cases, LES/FDF is more expensive than conventional LES. The overhead in comparison to non-FDF methods is expected, considering all of the SGS statistical information that LES/FDF provides. The computational time for FDF is significantly less than that of DNS. It is not claimed that LES/FDF is an alternative to DNS; nor is it claimed that FDF is capable of reproducing all DNS results, but this comparison could be done for cases where DNS was possible. The close proximity of values obtained by LES/FDF and DNS and the substantially lower computational costs of FDF make it a viable tool for simulations of reacting flow systems for which DNS is not possible. With the development of more efficient FDF solvers, it is predicted that LES/FDF will distinguish itself as a major tool for prediction of engineering combustion problems.

3 Interaction with AFRL

We are very grateful to have the opportunity of interacting with several of the researchers at the Wright-Patterson AFB on several occasions. The last time such interactions happened was in the summer of 2005, when the PI visited AFRL. Per recommendation of Dr. James Gord of AFRL/PR, the PI met with Drs. Vish Katta and Terry Meyer. The PI also met Dr. Datta Gaitonde of AFRL/VA and gave a tutorial/review seminar on SGS modeling in combustion for both AFRL/VA and AFRL/PR. This seminar was attended by more that 50 of AFRL scientists. It is obvious that the subject of LES is of significant interest at AFRL.

4 Enhancement of Technology and Education

With completion of this research, we have been able to contribute to maintain U.S. leadership in a technology which is of significant importance to DOD and AFOSR. In order to demonstrate our visibility in this research, here we shall list all the awards and some of noticeable achievements of the personnel involved in this program.

4.1 Graduate Students

Involvement of students in research is an issue which is taken very seriously at our University. We are committed to recruiting excellent quality students and involving them in high caliber research. During the past three years, the following students have been supported under this Grant.

1. Tomasz G. Drozda, Ph.D. in Mechanical Engineering, December 2005. Dissertation: Implementation of LES/SFMDF for Prediction of Non-Premixed Turbulent Flame. Current Position: Research Scientist, Combustion Research Facility, Sandia National Laboratories,, Livermore, CA.
2. Reza M.H. Sheikhi, Ph.D. in Mechanical Engineering, December 2005. Dissertation: Joint Velocity-Scalar Filtered Density Function for Large Eddy Simulation of Turbulent Reacting Flows. Current Position: Research Assistant Professor, the University of Pittsburgh, Pittsburgh, PA.

4.2 Awards and Honors

1. Peyman Givi received the NASA Public Service Medal: For contribution in the development of advanced modeling techniques for designing high-speed and hypersonic propulsion systems for aerospace vehicles (2005).

2. Peyman Givi was named Distinguished Alumnus, *Phi Kappa Phi* Honor Society, Youngstown State University, Youngstown, OH (2004).

3. Peyman Givi's Profile was featured in:

   - *Pittsburgh Tribune Review*, "Newsmaker," page B.2, September 8, 2005.
   - *Youngstown State University* Magazine, "An Outstanding Graduate", part of the article "60 Years of Engineering Excellence at YSU," pp. 22-23, Summer/Fall 2004.
   - *Technology Horizons:* "Aero Propulsion Combustors - A New Modeling Capability Quantitatively Predicts Aero Propulsion Combustor Performance," **5**(1), p. 46, February 2004.
   - *Pittsburgh Post-Gazette:* "Europe Slow in Stemming Brain Drain to America" and "Pittsburgh Brain Gain", **77**(81), October 20, 2003. Cover page and page A7.
   - *Space Directorate Highlights*, publication of NASA Glenn Research Center: Significant Research Finding: Sub-Grid Scale Modeling in Turbulent Combustion, June 21, 2003. Cleveland, OH.

4.3 Publications

In all of the following publications, the support from AFOSR is gratefully acknowledged:

Invited Review Articles and Book Chapters:

1. P. Givi, "Filtered Density Function for Subgrid Scale Modeling of Turbulent Combustion," *AIAA Journal*, **44**(1), 16–23 (2006).

2. P. Givi, "Subgrid Scale Modeling in Turbulent Combustion: A Review," AIAA Paper *2003-5081*, 2003.

3. C.K. Madnia, F.A. Jaberi and P. Givi "Large Eddy Simulation of Heat and Mass Transport in Turbulent Flows," Chapter 5 in *Handbook of Numerical Heat Transfer*, Second Edition, Editor: W.J. Minkowycz, E.M. Sparrow, and J.Y. Murthy, John Wiley & Sons, Inc., New York, NY, 2005.

Journal Articles in Print:

1. M.R.H. Sheikhi, T.G. Drozda, P. Givi, F.A. Jaberi and S.B. Pope, "Large Eddy Simulation of a Turbulent Nonpremixed Piloted Methane Jet Flame (Sandia Flame D)," *Proceedings of the Combustion Institute*, **30**, 549-556, 2005.

2. M.R.H. Sheikhi, T.G. Drozda, P. Givi and S.B. Pope, "Velocity-Scalar Filtered Density Function for Large Eddy Simulation of Turbulent Flows," *Physics of Fluids*, **15**(6), 2321-2337, 2003.

Conference Papers:

1. M.R.H. Sheikhi, P. Givi and S.B. Pope, "Implementation of the Velocity-Scalar Filtered Mass Density Function for Large Eddy Simulation of Turbulent Reacting Flows," *Bulletin of the American Physical Society*, **50**, p. 261, 58th Annual Meeting of the Division of Fluid Dynamics of the American Physical Society, Chicago, IL, November 20-22, 2005.

2. T.G. Drozda, M.R.H. Sheikhi, P. Givi and S.B. Pope, "Large Eddy Simulations of a Bluff-Body Stabilized Hydrogen-Methane Jet Flame' *Bulletin of the American Physical Society*, **50**, p. 101, 58th Annual Meeting of the Division of Fluid Dynamics of the American Physical Society, Chicago, IL, November 20-22, 2005.

3. Invited: P. Givi, "Quality Assessment of the Filtered Density Function for Large Eddy Simulation," Proceedings of the First Workshop on Quality Assessment of Unsteady Methods for Turbulent Combustion, Available on CD only, Darmstadt, Germany, June 16-17, 2005.

4. M.R.H. Sheikhi, P. Givi, and S.B. Pope, "Latest Developments in FDF Formulation," Proceedings of the Fourth Joint Meeting of the U.S. Sections of the Combustion Institute, available on CD only. Philadelphia, PA, March 20-23, 2005.

5. M.R.H. Sheikhi, P. Givi and S.B. Pope, "Joint Velocity-Scalar Filtered Mass Density Function for Large Eddy Simulation of Turbulent Reacting Flows," *Bulletin of the American Physical Society*, **49**(9), p. 217, 57th Annual Meeting of the Division of Fluid Dynamics of the American Physical Society, Seattle, WA, November 21-23, 2004.

6. P. Givi, M.R.H. Sheikhi, T.G. Drozda, and S.L. Yilmaz, "A New Strategy for Turbulence Simulation," Special Session on Multiscale Algorithms in Computational Fluid Dynamics, Meeting #1002 of the American Mathematical Society, Pittsburgh, PA, November 6-7, 2004.

7. T.G. Drozda, M.R.H. Sheikhi, P. Givi, F.A. Jaberi and S.B. Pope, "Scalar Filtered Density Function for Large Eddy Simulation of a Piloted Diffusion Flame," Session HT-10E, 2003 ASME International Mechanical Engineering Congress, Washington, D.C., November 15-21, 2003.

8. T.G. Drozda, M.R.H. Sheikhi, P. Givi, and S.B. Pope, "Large Eddy Simulation of Scalar Transport in a Turbulent Mixing Layer," Proceedings of the 2003 Fall Technical Meeting of the Combustion Institute, Eastern States Section, in *Chemical and Physical Processes in Combustion*, pp. 237-240, University Park, PA, October 26-29, 2003.

9. M.R.H. Sheikhi, T.G. Drozda, P. Givi, F.A. Jaberi, and S.B. Pope, "Large Eddy Simulation of Sandia Flame D," Proceedings of the 2003 Fall Technical Meeting of the Combustion Institute, Eastern States Section, in *Chemical and Physical Processes in Combustion*, pp. 241-244, University Park, PA, October 26-29, 2003.

Invited Public Lectures and Seminars:

During the course of this research, the PI delivered the following invited lectures and seminars.

1. Affordable and Reliable Prediction of Turbulent Combustion, Department of Mechanical Engineering, University of Utah, Salt Lake City, UT, February 3, 2006.

2. Affordable and Reliable Prediction of Turbulent Combustion, Computational Aerosciences Branch, NASA Langley Research Center, Hampton, VA, December 15, 2005.

3. Affordable and Reliable Prediction of Turbulent Combustion, The Center for 21st Century Energy, FALL 2005 Seminar Series, Department of Mechanical Engineering, Massachusetts Institute of Technology, Cambridge, MA, October 14, 2005.

4. Introduction to Simulation and Computational Fluid Dynamics, 16th International Activated Carbon Conference and Courses, Pittsburgh, PA, October 6, 2005.

5. LES of High Speed Combustion, The Media Effects Project, Presentation for Office of Secretary of Defense, NASA Langley Research Center, Hampton, VA, October 4, 2005.

6. Subgrid Scale Modeling for Large Eddy Simulation of Turbulent Reacting Flows: A Review, Institute for Scientific Computing, University of Wyoming, Laramie, WY, September 15, 2005.

7. Subgrid Scale Closure in Turbulent Combustion: A Review, Wright Patterson Air Force Base, AFRL/VA, Dayton, OH, August 24, 2005.

8. Filtered Mass Density Function for Subgrid Scale Modeling of Turbulent Diffusion Flames, ARO/AFOSR Contractors' Meeting in Chemical Propulsion, Indianapolis, IN, June 22, 2005.

9. Quality Assessment of the Filtered Density Function for Large Eddy Simulation, First Workshop on Quality Assessment of Unsteady Methods for Turbulent Combustion, Darmstadt, Germany, June 17, 2005.

10. Subgrid Scale Closure in Turbulent Combustion: A Review, CNRS, Ecole Centrale, Paris, France, June 13, 2005.

11. Subgrid Scale Closure in Turbulent Combustion: A Review, Colloquium of Sibley School of Mechanical and Aerospace Engineering," Cornell University, Ithaca, NY, March 29, 2005.

12. FDF and SPARK for LES, The Media Effects Project, Presentation for Office of Secretary of Defense, NASA Langley Research Center, Hampton, VA, March 11, 2005.

13. Mathematical Modeling and Computer Simulation of Combustion and Propulsion, Poster presented at the Energy Event: A Pitt Showcase of Energy Innovation, University of Pittsburgh, PA, December 9, 2004.

14. Implementation of FDF in SPARK-3D, The Media Effects Project, Presentation for Office of Secretary of Defense, NASA Langley Research Center, Hampton, VA, November 2, 2004.

15. Subgrid Scale Closure for Large Eddy Simulation of Turbulent Combustion, Advanced Analysis Processes, Rocketdyne Propulsion & Power, The Boeing Company, Canoga Park, CA, July 22, 2004.

16. Fire and Its Mystique: From the Caveman to the Rocket Scientist, Inaugural Lecture for Endowed WILLIAM KEPLER WHITEFORD Professorship, University of Pittsburgh, PA, February 19, 2004.

17. A New CFD Strategy for Simulation of Turbulence and Combustion, Center for Bioelectronics, Biosensors and Biochips, Department of Mechanical Engineering, Virginia Commonwealth University, Richmond, VA, December 10, 2003.

18. Supercomputer Simulations in Combustion and Propulsion: Making it Much Easier to be a Rocket Scientist, Poster presented at the Technology Commercialization Alliance, University of Pittsburgh, PA, December 9, 2003.

19. Subgrid Scale Modeling in Turbulent Combustion: A Review, 39th AIAA/ASME/SAE/ASEE Joint Propulsion Conference& Exhibit, Huntsville, AL, July 23, 2003.

20. Filtered Mass Density Function for Subgrid Scale Modeling of Turbulent Diffusion Flames, ARO/AFOSR Contractors' Meeting in Chemical Propulsion, Williamsburg, VA, June 25, 2003.

21. A Novel CFD Strategy for Turbulence and Combustion Simulation, Department of Mechanical and Industrial Engineering, University of Toronto, Toronto, Ontario, Canada, March 21, 2003.

22. Large Eddy Simulation of Turbulent Combustion, National Energy Technology Laboratory, U.S. Department of Energy, Morgantown, WV, February 11, 2003.

23. A Novel CFD Strategy for Turbulence Simulation, Institute for Complex Engineering Systems and Department of Mechanical Engineering, CMU, Pittsburgh, PA, January 24, 2003.

5 Acknowledgment

We are indebted to Professor Stephen B. Pope (Cornell University) for his valuable collaborations in various aspects of this work.

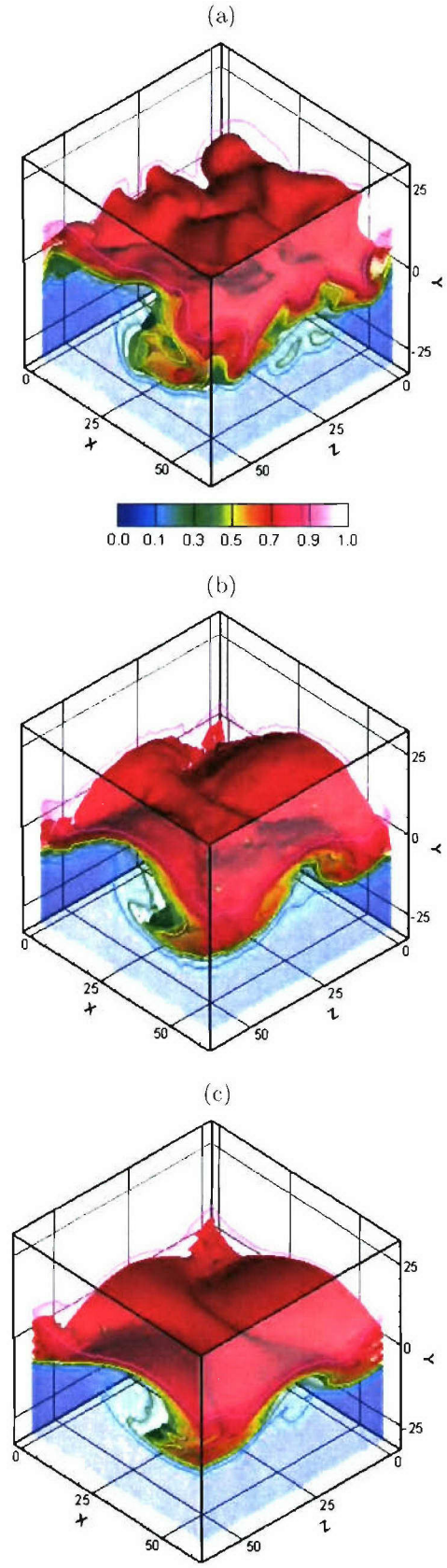

Figure 1: Contour surface of the $\langle \phi \rangle_L$ field in the 3D mixing layer at $t = 80$ as obtained by: (a) DNS, (b) VSFMDF and (c) Smagorinsky.

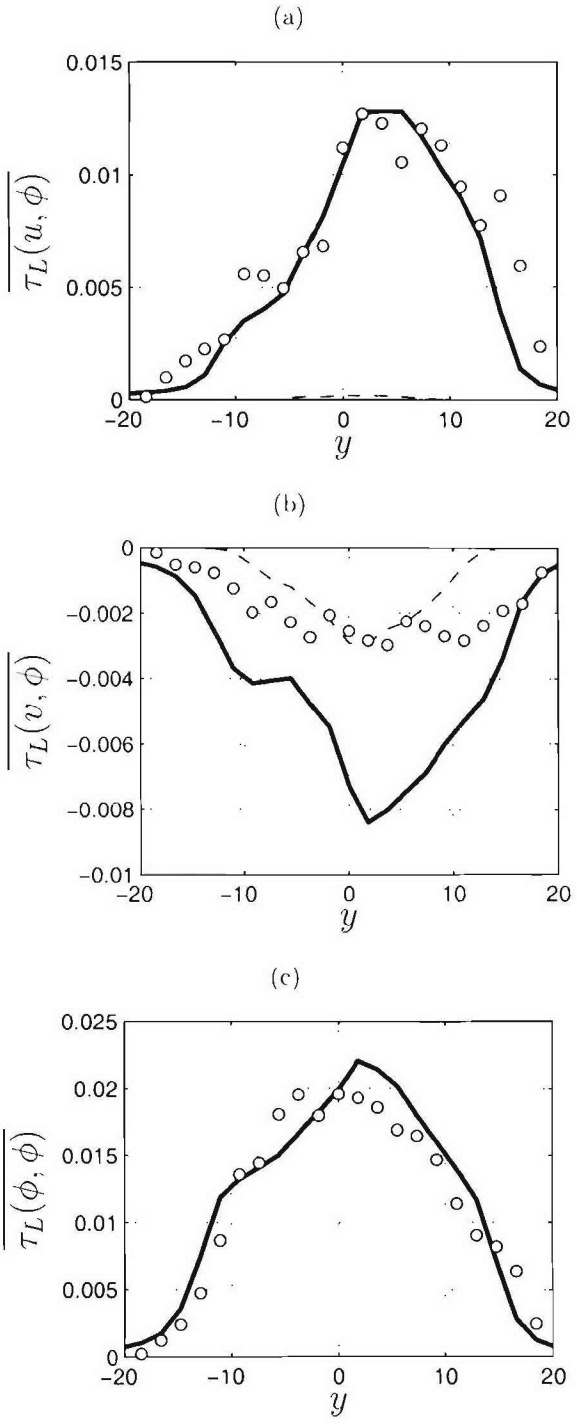

Figure 2: Cross-stream variations of some of the Reynolds-averaged components of τ_L at $t = 80$. The thick solid and thin dashed lines denote LES predictions using VSFMDF and Smagorinsky closures, respectively. The circles show the filtered DNS data.

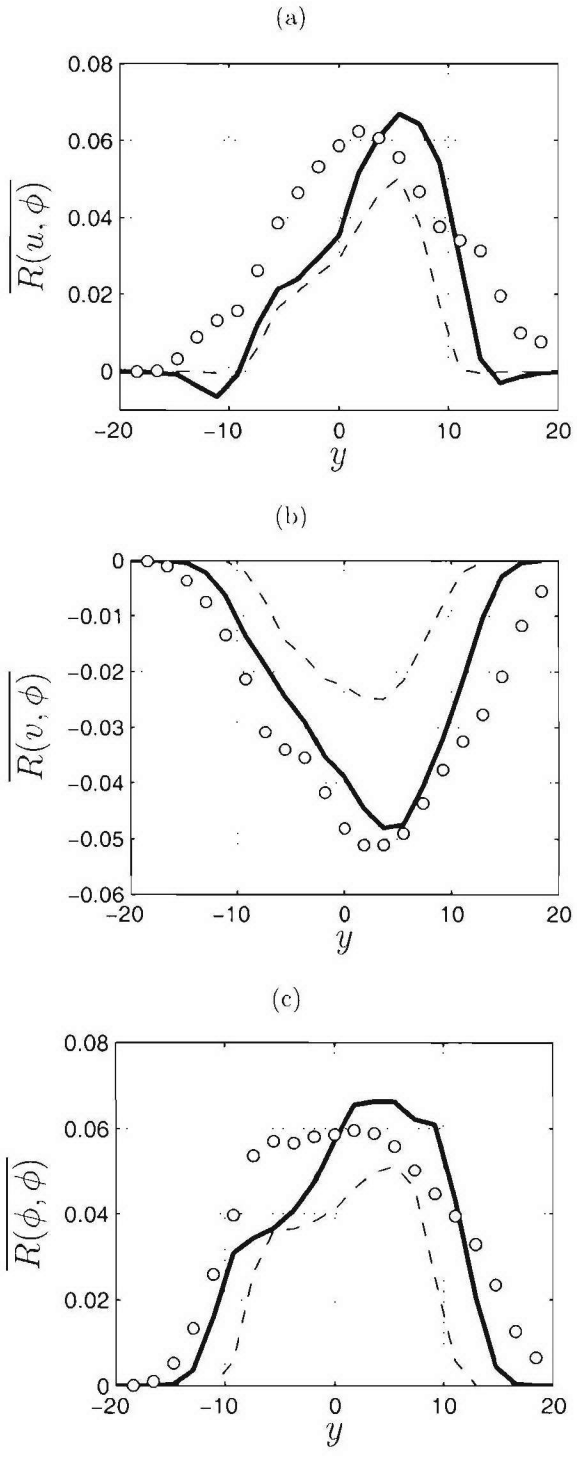

Figure 3: Cross-stream variations of some of the components of $\overline{R}$ at $t = 80$. The thick solid and thin dashed lines denote LES predictions using VSFMDF and Smagorinsky closures, respectively. The circles show the filtered DNS data.

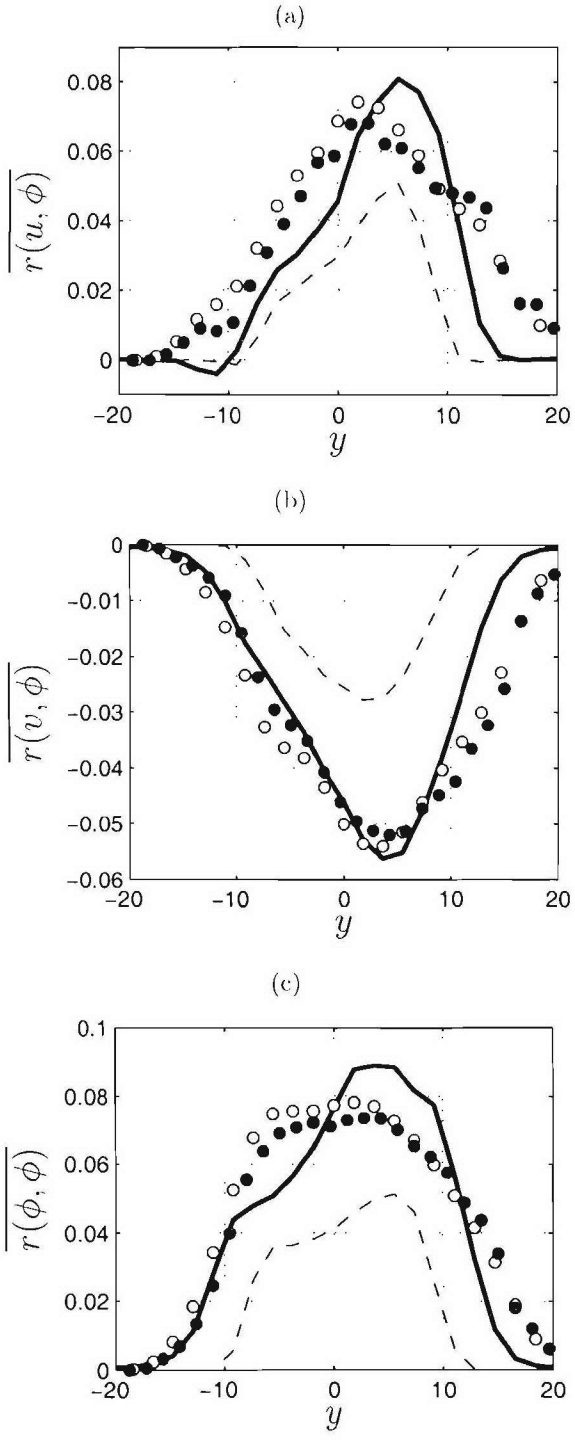

Figure 4: Cross-stream variations of $\overline{r}$ at $t = 80$. The thick solid and thin dashed lines denote LES predictions using VSFMDF and Smagorinsky closures, respectively. The white and black circles show the filtered and unfiltered DNS data, respectively.

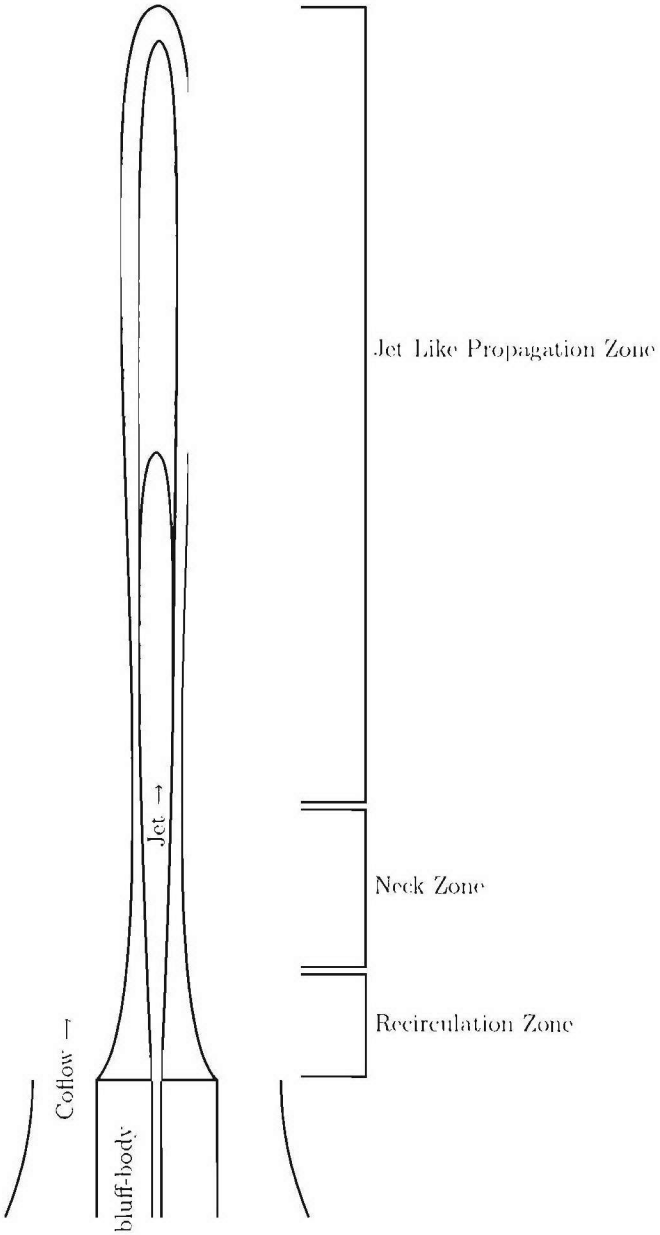

Figure 5: Sydney/Sandia bluff body flame configuration.

(a) B4C1-S1

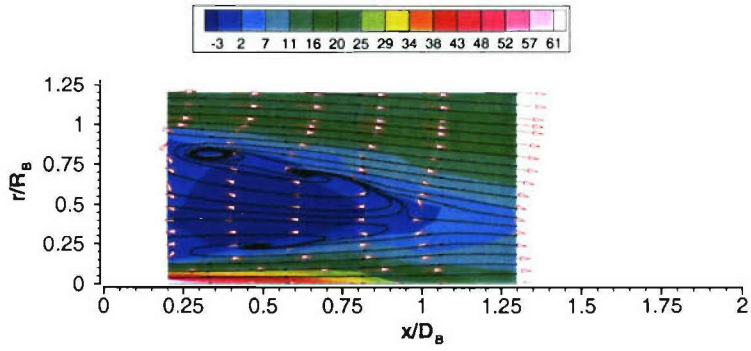

(b) B4C1-S2

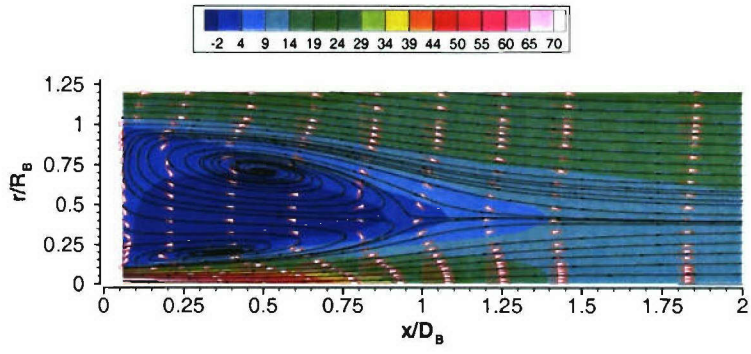

(c) B4C1-S3

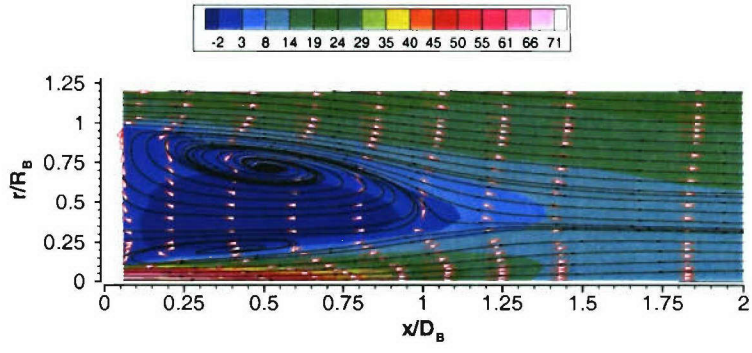

(d) LES-61

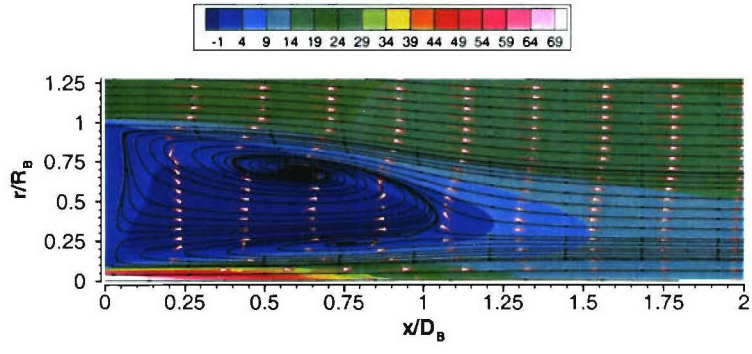

Figure 6: Time averaged recirculation features as predicted by experiments and LES. The color contours denote the streamwise velocity. Superimposed are the streamlines and the velocity vectors.

(a) LES-50

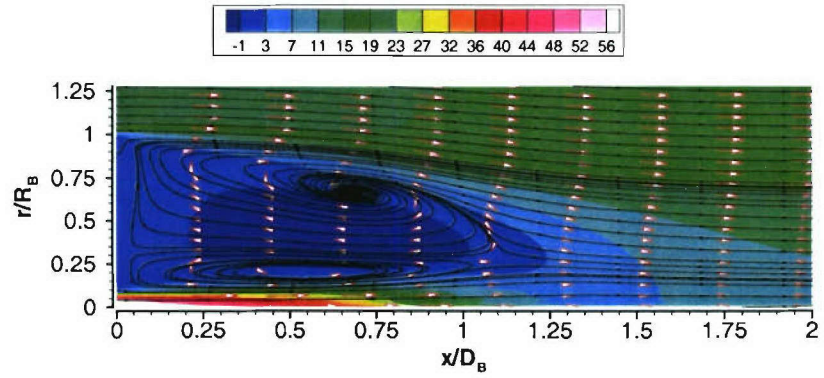

(b) LES-85

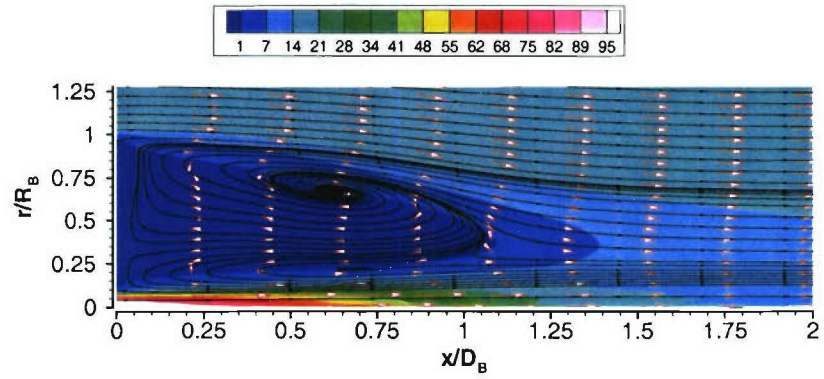

(c) LES-143

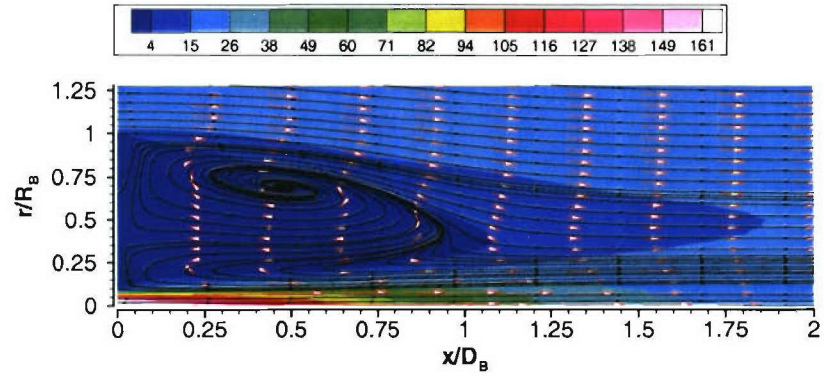

Figure 7: Time averaged recirculation features as predicted by LES. The color contours describe the streamwise velocity. Superimposed are the streamlines and the velocity vectors.

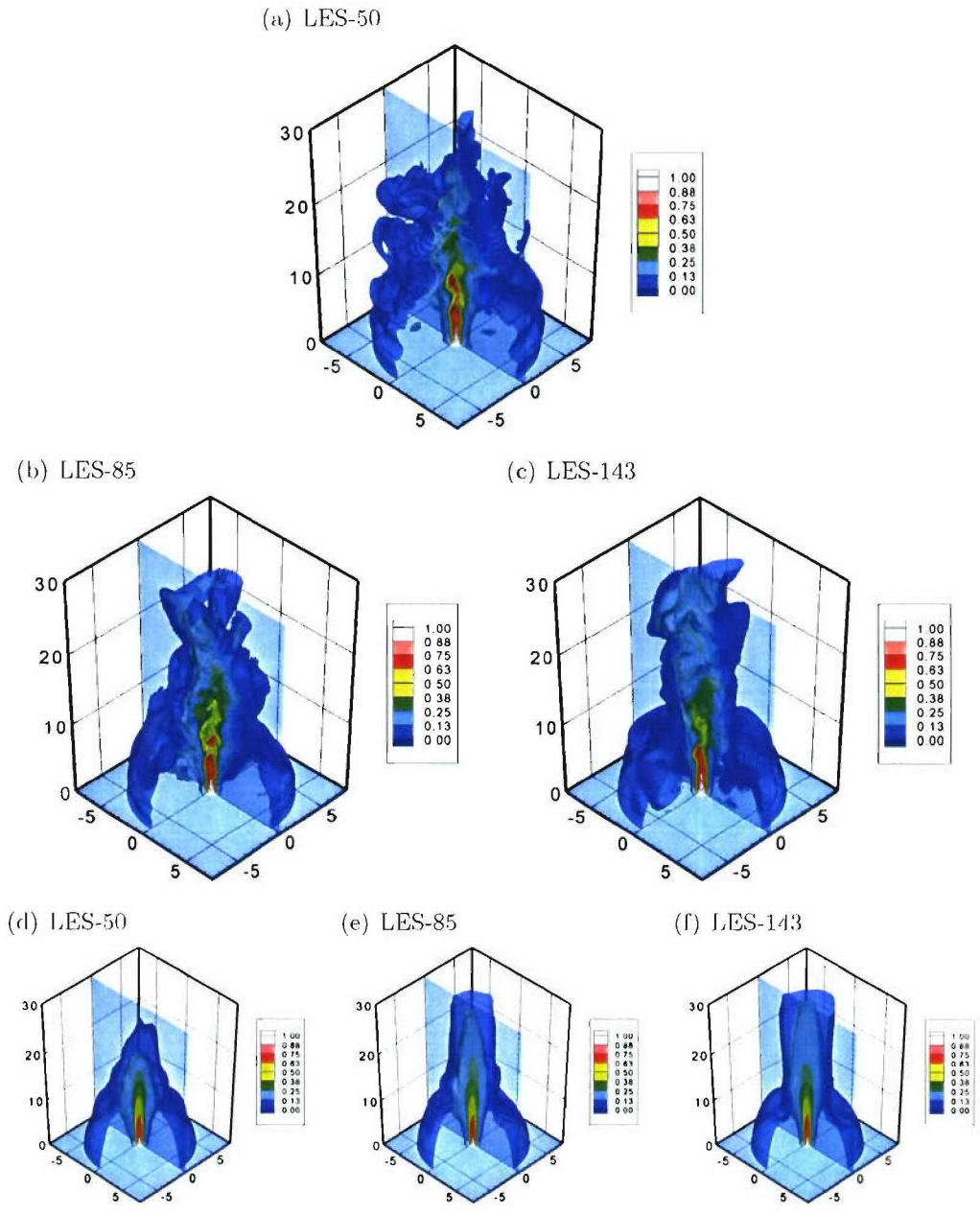

Figure 8: Instantaneous (a, b, c), and time averaged (d, e, f), contours of the mixture fraction as predicted by LES of several non-reacting flow configurations. The six iso-surfaces are 0.06 (blue), 0.13, 0.34, 0.45, 0.63, 0.90 (white). The plot's axes are normalized by the diameter of the fuel stream.

(a) HM1

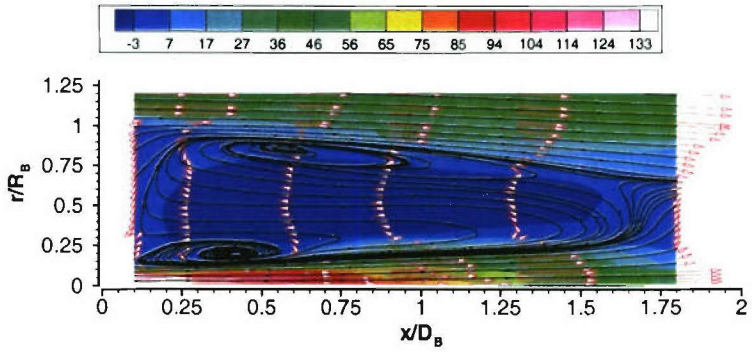

(b) HM1E-S1

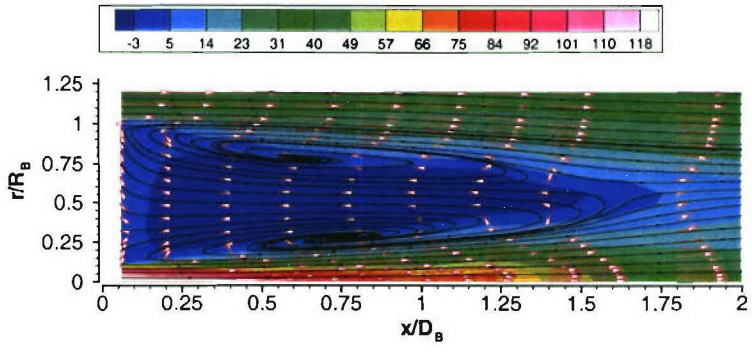

(c) HM1E-S2

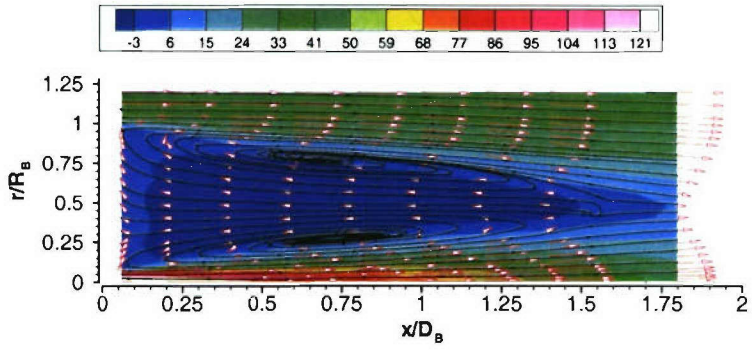

(d) LES/SFMDF

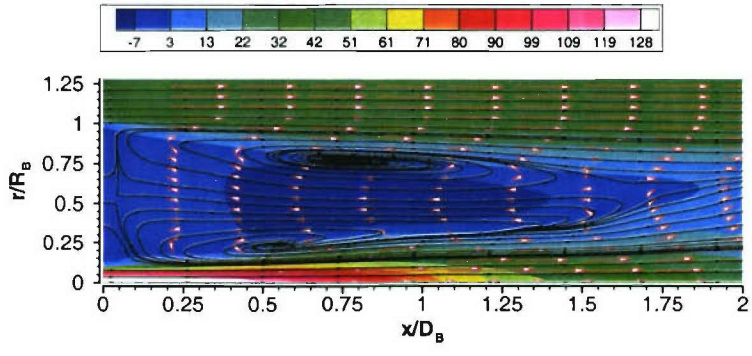

Figure 9: Time averaged recirculation features as predicted by SFMDF. The contours denote the streamwise velocity. Superimposed are the streamlines and the velocity vectors.

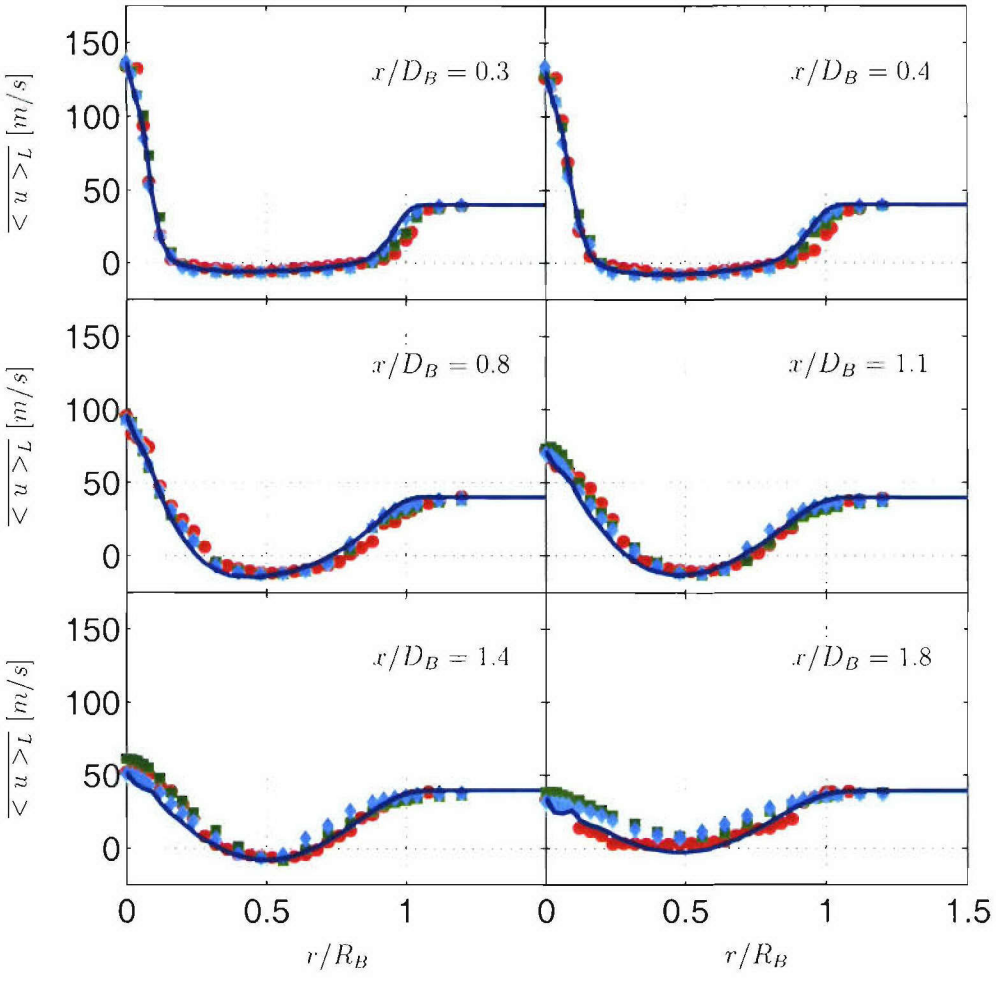

Figure 10: Radial profiles of the mean value of the streamwise velocity for the reacting flow. — SFMDF, • HM1, ■ HM1E-S1, ♦ HM1E-S2.

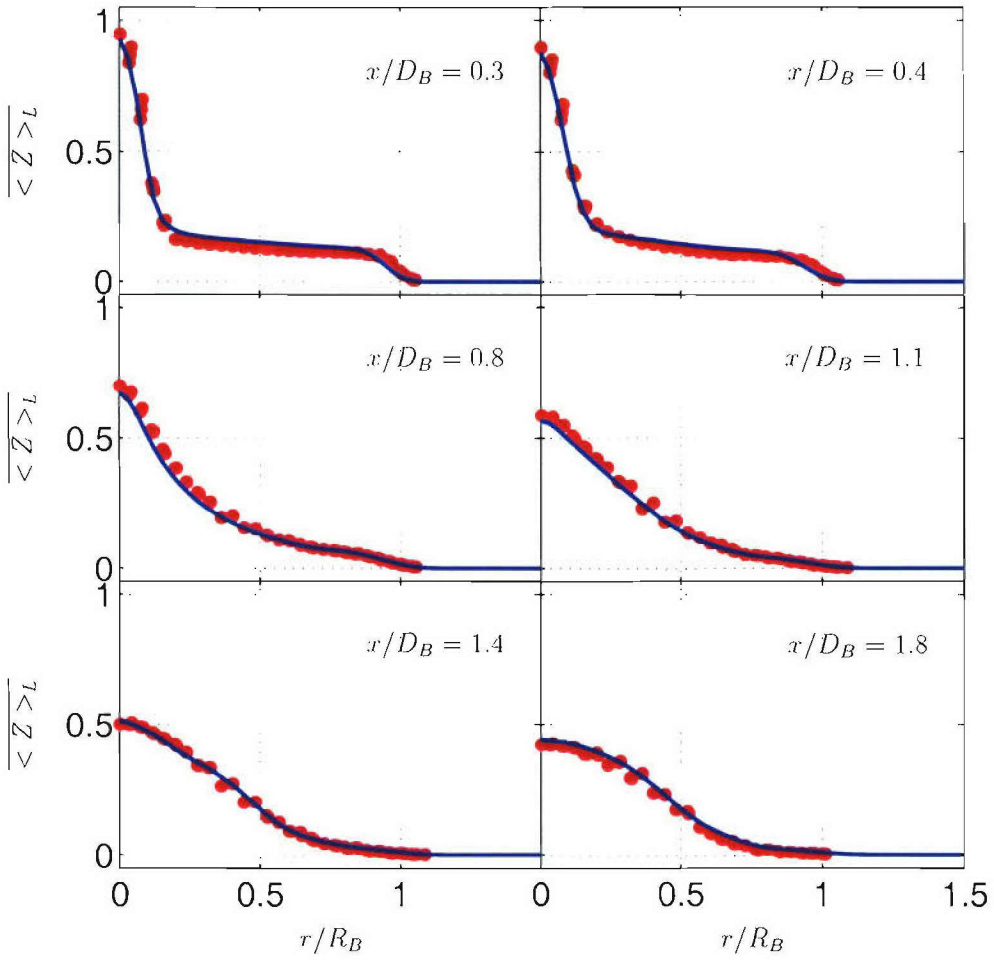

Figure 11: Radial profiles of the mean values of the mixture fraction for the reacting flow. — SFMDF, • HM1.

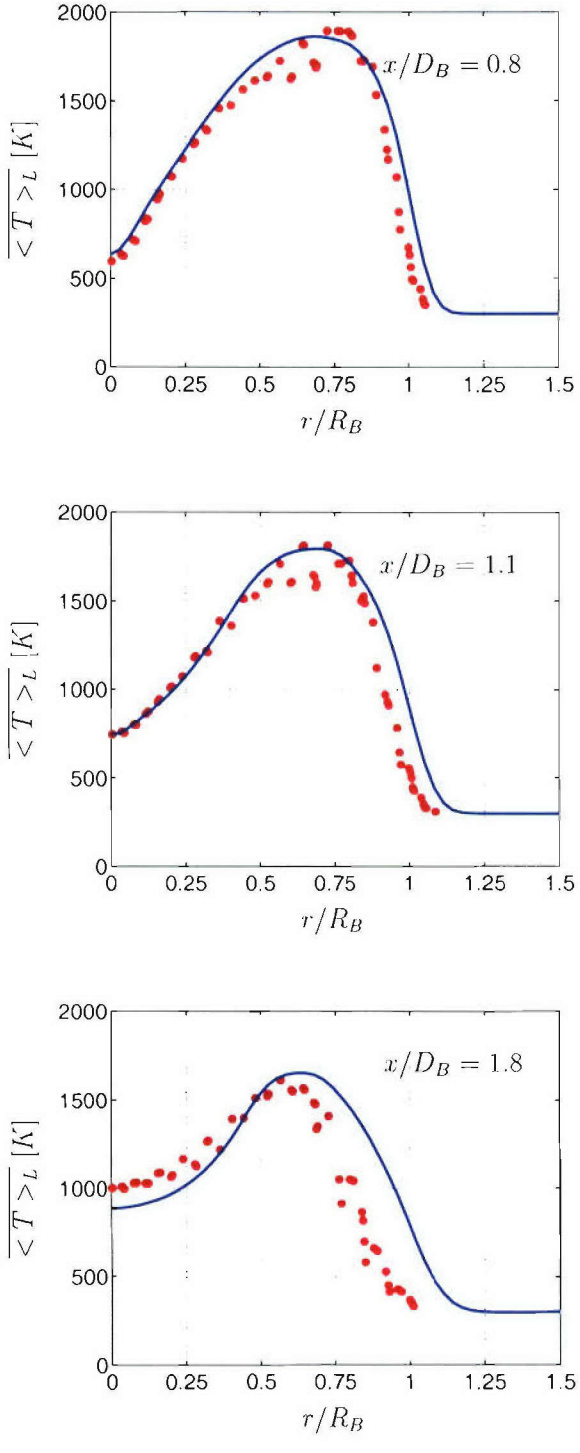

Figure 12: Radial profiles of the mean values of the temperature for the reacting flow. — SFMDF, • HM1.

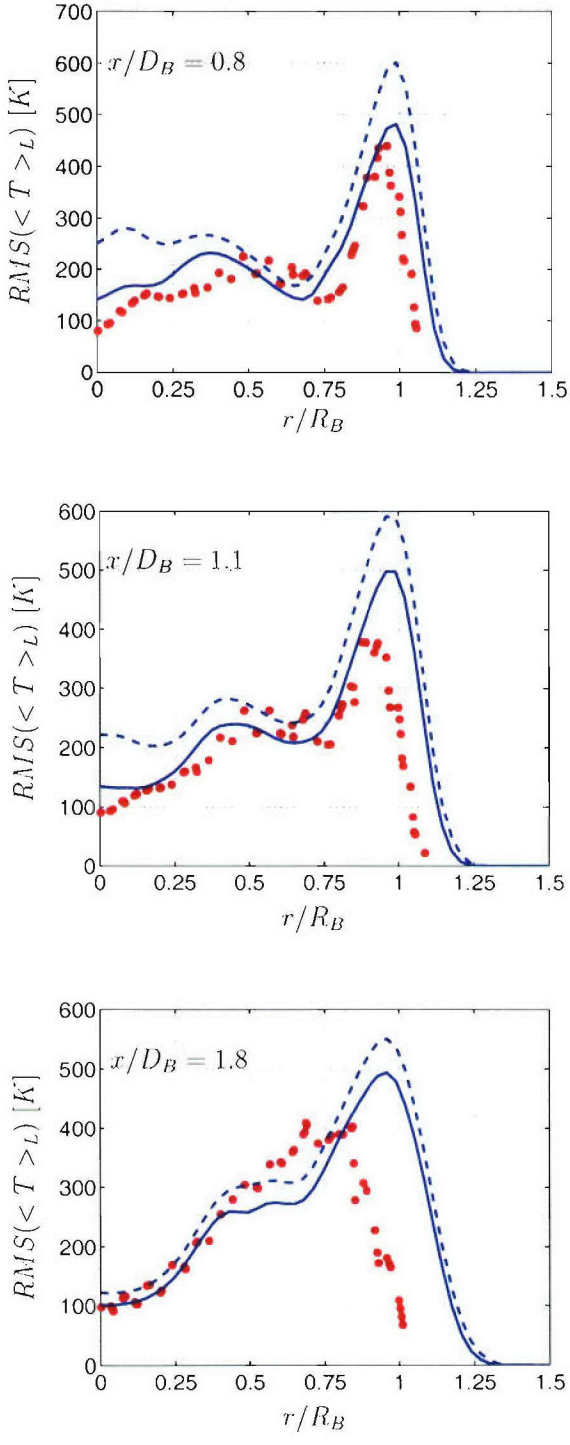

Figure 13: Radial profiles of the RMS values of the temperature for the reacting flow. —— Resolved SFMDF, - - - Total SFMDF, • HM1.

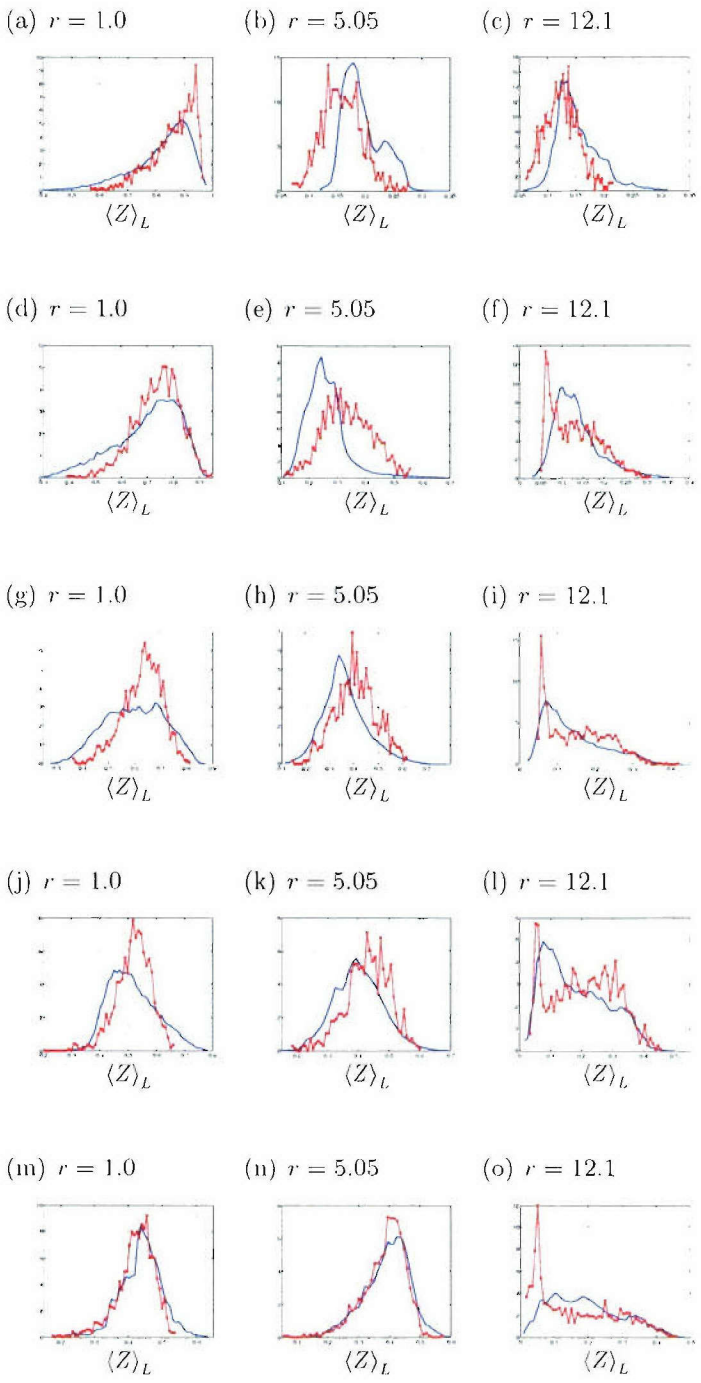

Figure 14: PDFs of the resolved mixture fraction at (top-to-bottom rows) $x/D_B = 0.3,\ 0.6,\ 0.9,\ 1.3,\ 1.8$ and selected radial locations (r $[mm]$). —— SFMDF, —●— HM1.

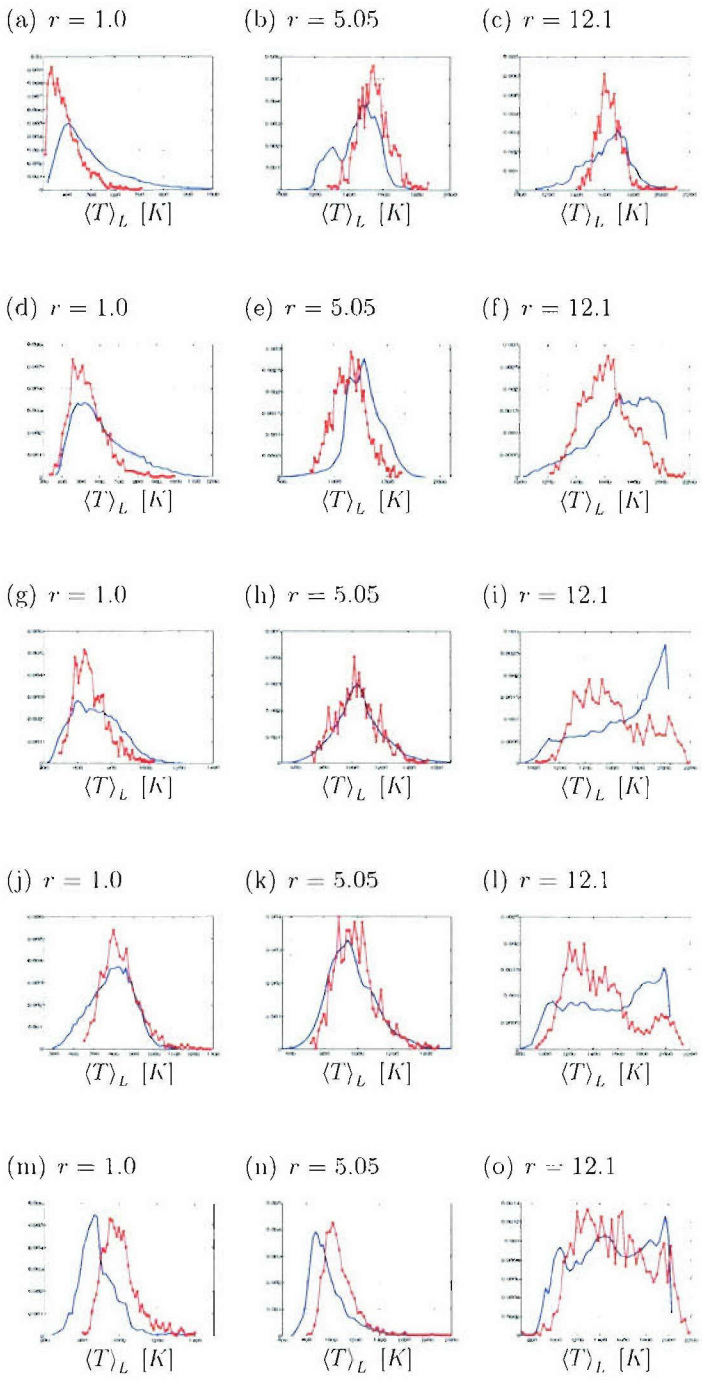

Figure 15: PDFs of the resolved temperature at (top-to-bottom rows) x/D_B = 0.3, 0.6, 0.9, 1.3, 1.8 and selected radial locations (r [mm]). —— SFMDF, —●— HM1.

References

1. Sandia National Laboratories, TNF Workshop website. `http://www.ca.sandia.gov/TNF/` (2005).
2. University of Sydney, Thermal Research Group website, Bluff-Body Flames. `http://www.mech.eng.usyd.edu.au/thermofluids/bluff.htm` (2005).
3. Bilger, R. W., Molecular transport effects in turbulent diffusion flames at moderate Reynolds number. *AIAA J.* **20** (1982) 962–970.
4. Bilger, R. W., Future progress in turbulent combustion research. *Prog. Energy Combust. Sci.* **26**(4-6) (2000) 367–380.
5. Bilger, R. W., Pope, S. B., Bray, K. N. C. and Driscoll, J. F., Paradigms in turbulent combustion research. *Proc. Combust. Inst.* **30** (2005) 21–42.
6. Bowman, C. T., Hanson, R. K., Gardiner, W. C., Lissianski, V., Frenklach, M., Goldenberg, M., Smith, G. P., Crosley, D. R. and Golden, D. M., GRI-mech 2.11–an optimized detailed chemical reaction mechanism for methane combustion and NO formation and reburning. Report GRI-97/0020, Gas Research Institute, Chicago, IL (1997).
7. Carpenter, M. H., A high-order compact numerical algorithm for supersonic flows. In: Morton, K. W. (ed.), *Twelfth International Conference on Numerical Methods in Fluid Dynamics*, vol. 371 of *Lecture Notes in Physics*, New York, NY: Springer-Verlag (1990), pp. 254–258.
8. Cha, C. M. and Troullet, P., A subgrid-scale mixing model for large-eddy simulations of turbulent reacting flows using the filtered density function. *Phys. Fluids* **15**(6) (2003) 1496–1504.
9. Chandy, A., Goldin, G. M. and Frankel, S. H., Modeling turbulent nonpremixed jet flames using Fluent's PDF transport model: Effect of mixing model on flame extinction. In: *30th International Symposium on Combustion, Abstracts of Work-In-Progress Posters*, Pittsburgh, PA: The Combustion Institute (2004), p. 447.
10. Colucci, P. J., Jaberi, F. A., Givi, P. and Pope, S. B., Filtered density function for large eddy simulation of turbulent reacting flows. *Phys. Fluids* **10**(2) (1998) 499–515.
11. Cook, A. W. and Riley, J. J., A subgrid model for equilibrium chemistry in turbulent flows. *Phys. Fluids* **6**(8) (1994) 2868–2870.
12. Dally, B. B., Fletcher, D. F. and Masri, A. R., Modelling of turbulent flames stabilised on a bluff-body. *Combust. Theor. Model.* **2** (1998) 193–219.
13. Dally, B. B., Masri, A. R., Barlow, R. S. and Fiechtner, G. J., Instantaneous and mean compositional structure of bluff-body stabilized nonpremixed flames. *Combust. Flame* **114** (1998) 119–148.

14. Dally, B. B., Masri, A. R., Barlow, R. S., Fiechtner, G. J. and Fletcher, D. F. In: *Proceedings of 26th Symp.(Int.) on Combustion*, Pittsburgh, PA: The Combustion Institute (1996).

15. DesJardin, P. E. and Frankel, S. H., Large eddy simulation of a turbulent nonpremixed reacting jet: Application and assessment of subgrid-scale combustion models. *Phys. Fluids* **10**(9) (1998) 2298–2314.

16. DesJardin, P. E. and Frankel, S. H., Two-dimensional large eddy simulation of soot formation in the near-field of a strongly radiating nonpremixed acetylene-air turbulent jet flame. *Combust. Flame* **119** (1999) 121–132.

17. Dreeben, T. D. and Pope, S. B., Probability density function and Reynolds-stress modeling of near-wall turbulent flows. *Phys. Fluids* **9**(1) (1997) 154–163.

18. Forkel, H. and Janicka, J., Large-eddy simulation of a turbulent hydrogen diffusion flame. *Flow Turbul. Combust.* **65**(2) (2000) 163–175.

19. Fox, R. O., *Computational Models for Turbulent Reacting Flows.* Cambridge, UK: Cambridge University Press (2003).

20. Frankel, S. H., Adumitroaie, V., Madnia, C. K. and Givi, P., Large eddy simulations of turbulent reacting flows by assumed PDF methods. In: Ragab, S. A. and Piomelli, U. (eds.), *Engineering Applications of Large Eddy Simulations*, New York, NY: ASME, FED-Vol. 162 (1993), pp. 81–101.

21. Gaffney, R. L., White, J. A., Girimaji, S. S. and Drummond, J. P., Modeling of temperature and species fluctuations in turbulent, reacting flow. *Computing Systems in Engineering* **5**(2) (1994) 117–113.

22. Geurts, B. J. (ed.), *Modern Simulation Strategies for Turbulent Flow.* Philadelphia, PA: R. T. Edwards, Inc. (2001).

23. Gicquel, L. Y. M., Givi, P., Jaberi, F. A. and Pope, S. B., Velocity filtered density function for large eddy simulation of turbulent flows. *Phys. Fluids* **14**(3) (2002) 1196–1213.

24. Givi, P., Model free simulations of turbulent reactive flows. *Prog. Energy Combust. Sci.* **15** (1989) 1–107.

25. Givi, P., Filtered density function for subgrid scale modeling of turbulent combustion. *AIAA J.* **44**(1) (2006) 16–23.

26. Glaze, D. J., Frankel, S. H. and Hewson, J. C., Non-premixed turbulent jet mixing using LES with the FMDF model. In: *30th International Symposium on Combustion, Abstracts of Work-In-Progress Posters*, Pittsburgh, PA: The Combustion Institute (2004), p. 79.

27. Grigoriu, M., *Applied Non-Gaussian Processes.* Englewood Cliffs, NJ: Prentice-Hall (1995).

28. Haworth, D. C. and Pope, S. B., A Generalized Langevin Model for turbulent flows. *Phys. Fluids* **29**(2) (1986) 387–405.

29. Haworth, D. C. and Pope, S. B., A second-order Monte Carlo method for the solution of the Ito stochastic differential equation. *Stochastic Analysis and Applications* **4**(2) (1986) 151–186.

30. Haworth, D. C. and Pope, S. B., Monte Carlo solutions of a joint PDF equation for turbulent flows in general orthogonal coordinates. *J. Comp. Phys.* **72**(2) (1987) 311–346.

31. Heinz, S., On Fokker-Planck equations for turbulent reacting flows. Part 2. Filtered density function for large eddy simulation. *Flow Turbul. Combust.* **70** (2003) 153–181.

32. Heinz, S., *Statistical Mechanics of Turbulent Flows.* New York, NY: Springer-Verlag (2003).

33. Hossain, M., Jones, J. C. and Malalasekera, W., Modelling of a bluff-body nonpremixed flame using a coupled radiation/flamelet combustion model. *Flow Turbul. Combust.* **67** (2001) 217–240.

34. Jaberi, F. A., Colucci, P. J., James, S., Givi, P. and Pope, S. B., Filtered mass density function for large eddy simulation of turbulent reacting flows. *J. Fluid Mech.* **401** (1999) 85–121.

35. Jaberi, F. A., Miller, R. S., Madnia, C. K. and Givi, P., Non-Gaussian scalar statistics in homogeneous turbulence. *J. Fluid Mech.* **313** (1996) 241–282.

36. James, S. and Jaberi, F. A., Large scale simulations of two-dimensional nonpremixed methane jet flames. *Combust. Flame* **123** (2000) 465–487.

37. Janicka, J. and Sadiki, A., Large eddy simulation of turbulent combustion systems. *Proc. Combust. Inst.* **30** (2005) 537–547.

38. Jenny, P., Muradoglu, K., Liu, K., Pope, S. B. and Caughey, D. A., PDF simulations of a bluff-body stabilized flow. *J. Comp. Phys.* **169** (2001) 1–23.

39. Jiménez, J., Liñán, A., Rogers, M. M. and Higuera, F. J., *A priori* testing of subgrid models for chemically reacting non-premixed turbulent flows. *J. Fluid Mech.* **349** (1997) 149–171.

40. Kempf, A., Forkel, H., Chen, J. Y., Sadiki, A. and Janicka, J., Large-eddy simulation of a counterflow configuration with and without combustion. *Proc. Combust. Inst.* **28** (2000) 35–40.

41. Kennedy, C. A. and Carpenter, M. H., Several new numerical methods for compressible shear-layer simulations. *Appl. Num. Math.* **14** (1994) 397–433.

42. Kloeden, P. E., Platen, E. and Schurz, H., *Numerical Solution of Stochastic Differential Equations through Computer Experiments.* New York, NY: Springer-Verlag, corrected second printing edn. (1997).

43. Kuan, T. S. and Lindstedt, R. P., Transported probability density function modeling of a bluff body stabilized turbulent flame. *Proc. Combust. Inst.* **30**(1) (2005) 767–774.

44. Libby, P. A. and Williams, F. A. (eds.), *Turbulent Reacting Flows*, vol. 44 of *Topics in Applied Physics*. Heidelberg: Springer-Verlag (1980).

45. Lin, S. J. and Corcos, G. M., The mixing layer: Deterministic models of a turbulent flow. Part 3. The effect of plane strain on the dynamics of streamwise vortices. *J. Fluid Mech.* **141** (1984) 139–178.

46. Liu, K., Pope, S. B. and Caughey, D. A., Calculations of bluff-body stabilized flames using a joint probablity density function model with detailed chamistry. *Combust. Flame* **141** (2005) 89–117.

47. Madnia, C. K. and Givi, P., Direct numerical simulation and large eddy simulation of reacting homogeneous turbulence. In: Galperin, B. and Orszag, S. A. (eds.), *Large Eddy Simulations of Complex Engineering and Geophysical Flows*, chap. 15, Cambridge, England: Cambridge University Press (1993), pp. 315–346.

48. Masri, A. R., Dally, B. B., Barlow, R. S. and Carter, C. D., The structure of the recirculation zone of a bluff-body combustor. *Proc. Combust. Inst.* **25** (1994) 1301–1308.

49. Masri, A. R., Dibble, R. W. and Barlow, R. S., Raman-Rayleigh measurements in bluff body stabilized flames of hydrocarbon fuels. *Proc. Combust. Inst.* **24** (1992) 317–324.

50. Masri, A. R., Dibble, R. W. and Barlow, R. S., The structure of turbulent nonpremixed flames revealed by Raman-Rayleigh-LIF measurements. *Prog. Energy Combust. Sci.* **22** (1996) 307–362.

51. Masri, A. R., Pope, S. B. and Dally, B. B., PDF computations of a strongly swirling nonpremixed flame stabilised on a new burner. *Proc. Combust. Inst.* **28** (2000) 123–131.

52. Meneveau, C. and Katz, J., Scale-invariance and turbulence models for large-eddy simulations. *Annu. Rev. Fluid Mech.* **32** (2000) 1–32.

53. Metcalfe, R. W., Orszag, S. A., Brachet, M. E., Menon, S. and Riley, J. J., Secondary instabilities of a temporally growing mixing layer. *J. Fluid Mech.* **184** (1987) 207–243.

54. Moser, R. D. and Rogers, M. M., The three-dimensional evolution of a plane mixing layer: The Kelvin-Helmholtz rollup. *J. Fluid Mech.* **243** (1992) 183–226.

55. Moser, R. D. and Rogers, M. M., Spanwise scale selection in plane mixing layers. *J. Fluid Mech.* **247** (1993) 321–337.

56. Moser, R. D. and Rogers, M. M., The three-dimensional evolution of a plane mixing layer: Pairing and transition to turbulence. *J. Fluid Mech.* **247** (1993) 275–320.

57. Muradoglu, M., Jenny, P., Pope, S. B. and Caughey, D. A., A consistent hybrid-volume/particle method for the PDF equations of turbulent reactive flows. *J. Comp. Phys.* **154**(2) (1999) 342–371.

58. Muradoglu, M., Liu, K. and Pope, S. B., PDF modeling of a bluff-body stabilized turbulent flame. *Combust. Flame* **132** (2003) 115–137.

59. Muradoglu, M., Pope, S. B. and Caughey, D. A., The hybrid method for the PDF equations of turbulent reactive flows: Consistency conditions and correction algorithms. *J. Comp. Phys.* **172** (2001) 841–878.

60. O'Brien, E. E., The probability density function (PDF) approach to reacting turbulent flows. In: Libby and Williams [44], chap. 5, pp. 185–218.

61. Peters, N., Laminar flamelet concepts in turbulent combustion. *Proc. Combust. Inst.* **21** (1986) 1231–1250.

62. Peters, N., *Turbulent Combustion.* Cambridge, UK: Cambridge University Press (2000).

63. Piomelli, U., Large-eddy simulation: Achievements and challenges. *Progress in Aerospace Sciences* **35** (1999) 335–362.

64. Pope, S. B., PDF methods for turbulent reactive flows. *Prog. Energy Combust. Sci.* **11** (1985) 119–192.

65. Pope, S. B., Computations of turbulent combustion: Progress and challenges. *Proc. Combust. Inst.* **23** (1990) 591–612.

66. Pope, S. B., Particle method for turbulent flows: Integration of stochastic model equations. *J. Comp. Phys.* **117** (1995) 332–349.

67. Pope, S. B., *Turbulent Flows.* Cambridge, UK: Cambridge University Press (2000).

68. Raman, V., Fox, R. O. and Harvey, A. D., Hybrid finite-volume/transported PDF simulations of a partially premixed methane-air flame. *Combust. Flame* **136**(3) (2004) 327–350.

69. Raman, V. and Pitsch, H., Large-eddy simulation of a bluff-body-stabilized non-premixed flame using a recursive filter-refinement procedure. *Combust. Flame* **142**(4) (2005) 329–347.

70. Raman, V., Pitsch, H. and Fox, R. O., Hybrid large-eddy simulation/Lagrangian filtered density function approach for simulating turbulent combustion. *Combust. Flame* **143**(1-2) (2005) 56–78.

71. Réveillon, J. and Vervisch, L., Response of the dynamic LES model to heat release. *Phys. Fluids* **8**(8) (1996) 2248–2250.

72. Réveillon, J. and Vervisch, L., Subgrid-scale turbulent micromixing: Dynamic approach. *AIAA J.* **36**(3) (1998) 336–341.

73. Riley, J. J. and Metcalfe, R. W., Direct numerical simulations of a perturbed, turbulent mixing layer. AIAA Paper 80-0274 (1980).

74. Risken, H., *The Fokker-Planck Equation, Methods of Solution and Applications.* New York, NY: Springer-Verlag (1989).

75. Sagaut, P., *Large Eddy Simulation for Incompressible Flows.* New York, NY: Springer-Verlag (2001).

76. Sandham, N. D. and Reynolds, W. C., Three-dimensional simulations of large eddies in the compressible mixing layer. *J. Fluid Mech.* **224** (1991) 133–158.

77. Sheikhi, M. R. H., *Joint Velocity-Scalar Filtered Density Function for Large Eddy Simulation of Turbulent Reacting Flows.* Ph.D. Thesis, Department of Mechanical Engineering, University of Pittsburgh, Pittsburgh, PA (2005).

78. Sheikhi, M. R. H., Drozda, T. G., Givi, P., Jaberi, F. A. and Pope, S. B., Large eddy simulation of a turbulent nonpremixed piloted methane jet flame (Sandia Flame D). *Proc. Combust. Inst.* **30** (2005) 549–556.

79. Sheikhi, M. R. H., Drozda, T. G., Givi, P. and Pope, S. B., Velocity-scalar filtered density function for large eddy simulation of turbulent flows. *Phys. Fluids* **15**(8) (2003) 2321–2337.

80. Smagorinsky, J., General circulation experiments with the primitive equations. I. The basic experiment. *Monthly Weather Review* **91**(3) (1963) 99–164.

81. Smith, G. P., Golden, D. M., Frenklach, M., Moriarty, N. W., Eiteneer, B., Goldenberg, M., Bowman, C. T., Hanson, R., Song, S., Gardiner, W. C., Lissianski, V. and Qin, Z., `http://www.me.berkeley.edu/gri_mech`

82. Tong, C., Measurements of conserved scalar filtered density function in a turbulent jet. *Phys. Fluids* **13**(10) (2001) 2923–2937.

83. van Vliet, E., Derksen, J. J. and van den Akker, H. E. A., Turbulent mixing in a tubular reactor: Assessment of an FDF/LES approach. *AIChE J.* **51**(3) (2005) 725–739.

84. Vreman, B., Geurts, B. and Kuerten, H., Realizability conditions for the turbulent stress tensor in large-eddy simulation. *J. Fluid Mech.* **278** (1994) 351–362.

85. Vreman, B., Geurts, B. and Kuerten, H., Large-eddy simulation of the turbulent mixing layer. *J. Fluid Mech.* **339** (1997) 357–390.

86. Wang, D. and Tong, C., Conditionally filtered scalar dissipation, scalar diffusion, and velocity in a turbulent jet. *Phys. Fluids* **14**(7) (2002) 2170–2185.

87. Wang, D., Tong, C. and Pope, S. B., Experimental study of velocity filtered joint density function for large eddy simulation. *Phys. Fluids* **16**(10) (2004) 3599–3613.

88. Wouters, H. A., Peeters, T. W. J. and D., R., Joint velocity-scalar PDF methods. In: Launder, B. E. and Sandham, N. D. (eds.), *Closure Strategies for Turbulent and Transitional Flows*, Cambridge University Press (2002).

89. Xu, J. and Pope, S. B., Assessment of numerical accuracy of PDF/Monte Carlo methods for turbulent reacting flows. *J. Comp. Phys.* **152** (1999) 192–230.

90. Zhou, X. Y. and Pereira, J. C. F., Large eddy simulation (2D) of a reacting plan mixing layer using filtered density function. *Flow Turbul. Combust.* **64** (2000) 279–300.